

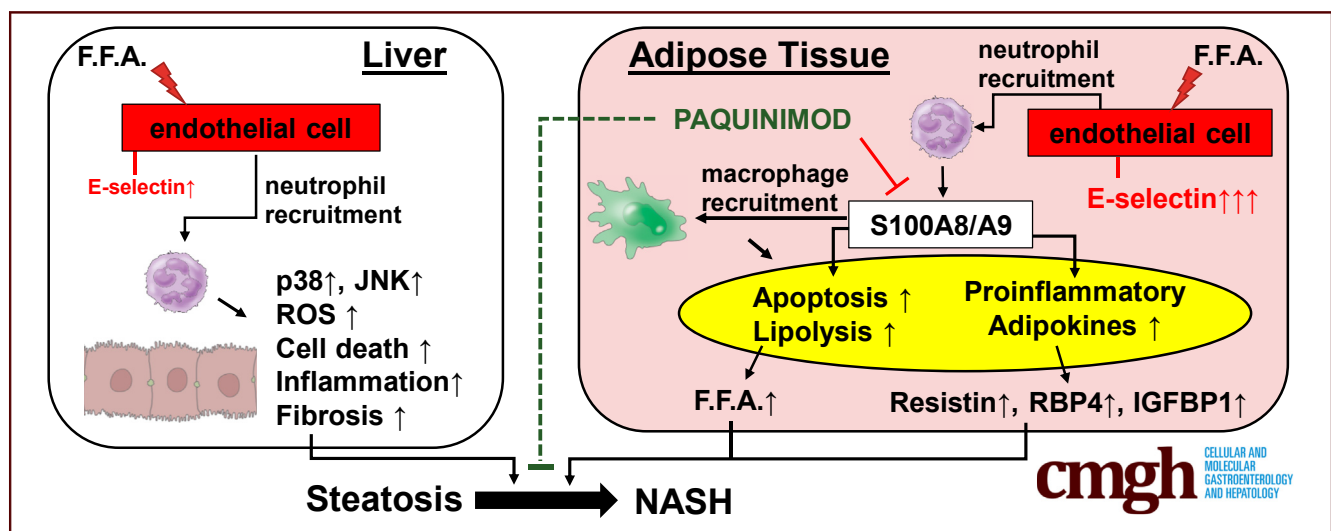
ORIGINAL RESEARCH

E-Selectin-Dependent Inflammation and Lipolysis in Adipose Tissue Exacerbate Steatosis-to-NASH Progression via S100A8/9



Robim M. Rodrigues,^{1,2} Yong He,¹ Seonghwan Hwang,¹ Adeline Bertola,¹ Bryan Mackowiak,¹ Yeni Ait Ahmed,¹ Wonhyo Seo,¹ Jing Ma,¹ Xiaolin Wang,¹ Seol Hee Park,¹ Yukun Guan,¹ Yaojie Fu,¹ Tamara Vanhaecke,² Dechun Feng,¹ and Bin Gao¹

¹Laboratory of Liver Diseases, National Institute on Alcohol Abuse and Alcoholism, National Institutes of Health, Bethesda, Maryland; ²Department of In Vitro Toxicology and Dermato-Cosmetology, Faculty of Medicine and Pharmacy, Vrije Universiteit Brussel, Brussels, Belgium



SUMMARY

E-selectin, a key adhesion molecule for neutrophils, is highly up-regulated in adipose tissue of nonalcoholic steatohepatitis patients compared with individuals with fatty liver. Deletion of the E-selectin gene or inhibition of neutrophil-derived S100A9 in mice ameliorated adipose tissue inflammation, improving nonalcoholic steatohepatitis.

BACKGROUND & AIMS: Nonalcoholic steatohepatitis (NASH) is a leading cause of chronic liver disease, characterized by steatosis and hallmark liver neutrophil infiltration. NASH also is associated with adipose tissue inflammation, but the role of adipose tissue inflammation in NASH pathogenesis remains obscure. The aim of this study was to investigate the interplay between neutrophil recruitment in adipose tissue and the progression of NASH.

METHODS: A mouse model of NASH was obtained by high-fat diet (HFD) feeding plus adenovirus-*Cxcl1* overexpression (HFD+*AdCxcl1*). Genetic deletion of E-selectin (*Sele*) and treatment with an S100A9 inhibitor (Paquinimod) were investigated using this model.

RESULTS: By analyzing transcriptomic data sets of adipose tissue from NASH patients, we found that E-selectin, a key

adhesion molecule for neutrophils, is the highest up-regulated gene among neutrophil recruitment-related factors in adipose tissue of NASH patients compared with those in patients with simple steatosis. A marked up-regulation of *Sele* in adipose tissue also was observed in HFD+*AdCxcl1* mice. The HFD+*AdCxcl1*-induced NASH phenotype was ameliorated in *Sele* knockout mice and was accompanied by reduced lipolysis and inflammation in adipose tissue, which resulted in decreased serum free fatty acids and proinflammatory adipokines. S100A8/A9, a major proinflammatory protein secreted by neutrophils, was highly increased in adipose tissue of HFD+*AdCxcl1* mice. This increase was blunted in the *Sele* knockout mice. Therapeutically, treatment with the S100A9 inhibitor Paquinimod reduced lipolysis, inflammation, and adipokine production, ameliorating the NASH phenotype in mice.

CONCLUSIONS: E-selectin plays an important role in inducing neutrophil recruitment in adipose tissue, which subsequently promotes inflammation and lipolysis via the production of S100A8/A9, thereby exacerbating the steatosis-to-NASH progression. Targeting adipose tissue inflammation therefore may represent a potential novel therapy for treatment of NASH. (*Cell Mol Gastroenterol Hepatol* 2022;13:151-171; <https://doi.org/10.1016/j.jcmgh.2021.08.002>)

Keywords: Nonalcoholic Fatty Liver Disease (NAFLD); Steatohepatitis; Neutrophils; Paquinimod; CXCL1.

Nonalcoholic fatty liver disease (NAFLD) encompasses a series of chronic liver disorders with varying injury severity ranging from simple steatosis to nonalcoholic steatohepatitis (NASH), cirrhosis, and hepatocellular carcinoma (HCC).¹ NASH is characterized by hepatic steatosis, lobular inflammation, hepatocyte damage, and, typically, also pericellular fibrosis. NASH can progress further into cirrhosis and eventually to primary hepatocellular carcinoma, posing a serious health risk.¹ It is estimated that NASH affects 1.5%–6.5% of the general population, and that figure is expected to dramatically increase in the next decade.^{2–4} The mechanisms involved in the transition of simple steatosis, which is mostly asymptomatic, toward NASH have not been fully elucidated. Our group previously showed that the hepatic infiltration of neutrophils plays a crucial role in promoting the steatosis-to-NASH transition.^{5–7} However, the contribution of adipose tissue to this so-called neutrophil-driven NASH has not been documented. Because a crosstalk between adipose tissue inflammation and the liver was suggested to be implicated in NASH development,^{8,9} we investigated in this study how neutrophil recruitment in adipose tissue may influence NASH.

Immune cell recruitment requires vascular endothelial cell activation and expression of adhesion molecules necessary for leukocyte extravasation from the vasculature to areas of inflammation.¹⁰ As per the leukocyte adhesion cascade paradigm (consisting of capture, rolling, arrest, adhesion, and transendothelial migration), the rolling of leukocytes is mediated by selectins. Therefore the regulated expression of selectins and their ligands initiate an inflammatory response.^{10–12} The selectin family consists of 3 cell adhesion molecules, namely L-selectin (SELL), which is expressed by most leukocytes, and E-selectin (SELE) and P-selectin (SELP), which are expressed by activated endothelial cells and interact with glycosylated ligands such as CD44 and SELP glycoprotein ligand 1.^{10,13}

We previously showed that chronic-binge ethanol feeding in mice up-regulates the hepatic expression of *Sele*, inducing hepatic neutrophil accumulation, injury, and inflammation.¹⁴ Deletion of the *Sele* gene reverted this process, preventing hepatic neutrophil infiltration and reducing alcohol-induced liver injury.¹⁴ This made us believe that E-selectin might also play a role in promoting the development of steatosis and NASH. We found that *SELE/Sele* messenger RNAs (mRNAs) indeed were up-regulated in human and mouse livers during NASH, compared with normal livers or steatotic livers. However, this up-regulation was much more pronounced in visceral adipose tissues than in liver tissues, which allowed us to hypothesize that E-selectin involvement in NASH progression was not exclusively in the liver, but also, and even predominantly, in adipose tissue. In the current study, we found that deletion of the *Sele* gene also reduced liver inflammation and injury in a mouse model of NASH induced by high-fat diet feeding plus adenovirus-*Cxcl1* overexpression


(HFD^{+AdCxcl1}).⁶ Interestingly, deletion of the *Sele* gene markedly reduced adipose tissue neutrophil recruitment and resulted in a decrease in lipolysis and secretion of free fatty acids (FFAs) and proinflammatory adipokines. Furthermore, we found that expression of S100A8 and S100A9 (also known as myeloid-related protein [MRP] 8 and MRP14, respectively), which are Ca²⁺-binding proteins and represent 40% of neutrophil cytosolic protein weight,^{15–18} is highly increased in adipose tissue in HFD^{+AdCxcl1}-induced NASH mice. The S100A8/A9 heterodimer released by activated neutrophils has been described as an innate immune mediator during the pathogenesis of multiple diseases,^{16,19,20} and higher expression of *S100A8* and *S100A9* have been documented in visceral adipose tissue of type 2 diabetic obese patients.²¹ However, the role of S100A8/A9 in steatosis-to-NASH progression has not been documented, although increased serum S100A8/A9 levels in NASH patients have been reported.²² In the current study, we found that an increase of S100A8 and S100A9 proteins in adipose tissue is dependent on E-selectin because this increase was reduced markedly in *Sele* knockout (KO) mice. Finally, administration of Paquinimod (PAQ), a small molecule that inhibits S100A9 by interacting with its corresponding receptors (ie, receptor for advanced glycation end products and Toll-like receptor 4),²³ significantly reduced adipose tissue lipolysis and liver injury in mice under NASH conditions, suggesting that inhibition of S100A9 proteins may represent a potential novel therapy against NASH.

Results

E-Selectin in Adipose Tissue Is Highly Up-regulated in Patients and Mice With NASH

Analysis of transcriptomic data sets of adipose tissue from NASH patients⁹ showed that among the neutrophil-recruitment genes, E-selectin (*SELE*) was the highest up-regulated gene in the adipose tissue of NASH, compared with adipose tissue from patients with steatosis or healthy livers (Figure 1A). The expression of other selectin molecules in the same cohorts was not (such as: *SELP*) or was only slightly (such as: *SELL*) increased during NASH. Furthermore, the induction of *VCAM1* *ICAM1*, which are adhesion molecules that play a role in later stages of the

Abbreviations used in this paper: AdCxcl1, adenovirus-Cxcl1; ALT, alanine aminotransferase; ANGPTL3, angiopoietin-like protein 3; AST, aspartate aminotransferase; CXCL1, C-X-C motif chemokine ligand 1; ELISA, enzyme-linked immunosorbent assay; FFA, free fatty acid; GTT, glucose tolerance test; HFD, high-fat diet; IGFBP1, insulin-like growth factor-binding protein 1; IL, interleukin; ITT, insulin tolerance test; KO, knockout; MPO, myeloperoxidase; mRNA, messenger RNA; MRP, myeloid-related protein; NAFLD, nonalcoholic fatty liver disease; NASH, nonalcoholic steatohepatitis; PAQ, Paquinimod; Rbp4, retinol binding protein 4; RT-qPCR, reverse-transcription quantitative polymerase chain reaction; SELE, E-selectin; SELL, L-selectin; SELP, P-selectin; TSEC, immortalized liver sinusoidal endothelial cell line; WT, wild-type.

 Most current article

© 2021 The Authors. Published by Elsevier Inc. on behalf of the AGA Institute. This is an open access article under the CC BY-NC-ND license (<http://creativecommons.org/licenses/by-nc-nd/4.0/>).

2352-345X

<https://doi.org/10.1016/j.jcmgh.2021.08.002>

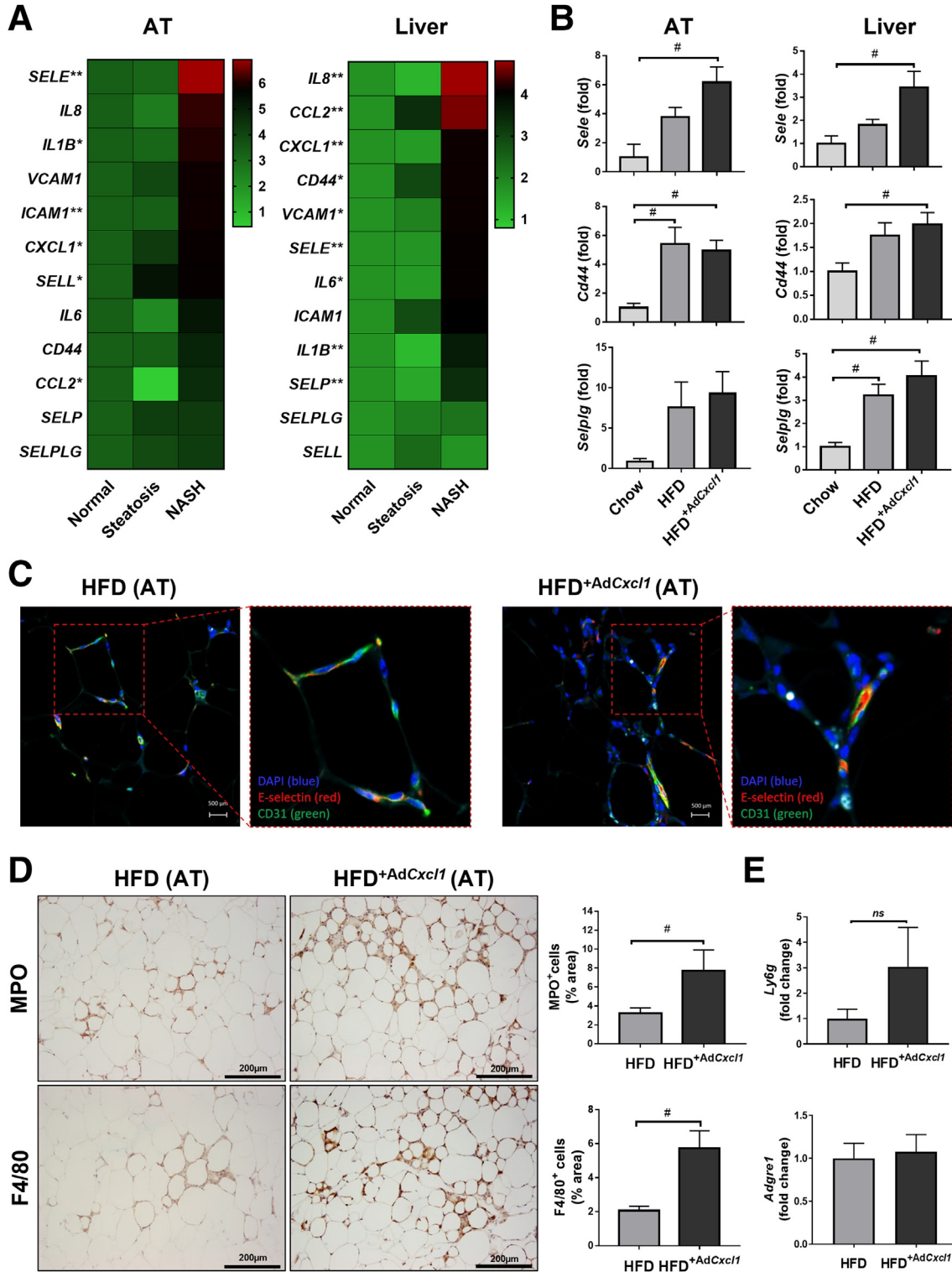


Figure 1. E-selectin is predominantly up-regulated in adipose tissue (AT) of patients and mice with NASH. (A) Normalized gene expression (microarray data sets obtained from Du Plessis et al⁹ and Lake et al²⁵) in visceral adipose tissue and liver (L) of patients suffering from steatosis ($n_{AT} = 6$, $n_L = 10$) and NASH ($n_{AT} = 13$, $n_L = 15$) compared with those from healthy controls ($n_{AT} = 8$, $n_L = 19$). (B–E) WT mice were subjected to chow diet (Chow) ($n = 7$), a 3-month high-fat diet plus AdGfp (HFD) ($n = 7$) to induce steatosis or 3-month HFD plus AdCxcl1 to induce NASH (HFD+AdCxcl1) ($n = 7$). Adipose and liver tissues were collected and analyzed. (B) RT-qPCR of adipose tissue and liver. (C) Immunofluorescence staining of E-selectin (red), CD31 (green), and 4',6-diamidino-2-phenylindole (DAPI) (blue) of adipose tissue. (D) MPO and F4/80 immunostaining of adipose tissues. (E) RT-qPCR of adipose tissue. * $P < .05$ for NASH vs normal, ** $P < .05$ for steatosis vs normal or NASH vs normal. # $P < .05$.

leukocyte adhesion cascade,¹⁰ were induced much less prominently than *SELE*. A trend in line with the *SELE* expression also was observed for the up-regulation of *CD44*, which encodes for a cell-surface glycoprotein that acts as the major E-selectin ligand²⁴ and for the up-regulation of SELP ligand. Interestingly, the expression of several inflammatory markers, including *CCL2*, C-X-C motif chemokine ligand 1 (*CXCL1*), and *IL1B*, were increased in adipose tissue from NASH patients compared with those from healthy controls or with fatty liver. As illustrated in Figure 1A (right panel), analysis of transcriptomic data sets of human NASH liver samples²⁵ showed that among the neutrophil-recruitment genes, *IL8* was the highest up-regulated gene in liver tissues from NASH, compared with samples from patients with steatosis or healthy livers. Hepatic *SELE* expression also was higher during NASH compared with steatosis or healthy livers, but not as prominently as in adipose tissue. Furthermore, hepatic expression of *VCAM1* and *SELP* also was up-regulated in the NASH cohort. However, the expression of *SELL* and *ICAM1* did not differ among patient groups. Interestingly, the expression of major inflammatory markers *CCL2*, *CXCL1*, *IL6*, and *IL1B* was increased in liver tissues from NASH patients compared with those from healthy controls or with fatty liver.

Next, we examined the expression of *Sele* in a HFD^{+AdCxcl1}-induced murine NASH model⁶ and found that *Sele* expression in the liver and adipose tissue also was up-regulated compared with HFD-fed mice injected with a control virus expressing green fluorescence protein (HFD^{+AdGFP}) (simple steatosis model) (Figure 1B). Such up-regulation was seen predominantly in visceral adipose tissue, although the liver also showed a significant *Sele* increase during NASH, indicating the similarity to human data. E-selectin ligands *Cd44* and *Selplg* also were up-regulated, although the latter did not reach significant levels in adipose tissue (Figure 1B). The increase of E-selectin in adipose tissue also was confirmed by immunofluorescence staining in which endothelial cells, labeled by CD31 (green) showed a higher expression of E-selectin (red) in adipose tissue from HFD^{+AdCxcl1} mice than those from HFD-fed mice (Figure 1C).

We previously reported that the number of neutrophils and macrophages was increased markedly in the liver tissues of HFD^{+AdCxcl1} mice compared with those from HFD-fed mice.⁶ Likewise, we found that adipose tissue from HFD^{+AdCxcl1} mice had greater neutrophil and macrophage infiltration than those from HFD-fed mice, as shown by immunostaining of myeloperoxidase (MPO) and F4/80 (Figure 1D), and by reverse-transcription quantitative polymerase chain reaction (RT-qPCR) analysis of the neutrophil marker *Ly6g*, although no increase in *Adgre1* expression, which codes for F4/80, was observed (Figure 1E).

To examine the correlation between *Sele* expression in activated endothelial cells and neutrophil recruitment, we performed in vitro experiments using an immortalized liver sinusoidal endothelial cell line (TSEC). Treatment with a range of cytokines, including interleukin (IL)1 β , tumor necrosis factor α , and transforming growth factor β , as well as cell culture supernatants of primary mouse hepatocytes

previously treated with palmitic acid, significantly up-regulated *Sele* mRNA levels in TSEC (Figure 2A). Palmitic acid treatment alone also up-regulated E-selectin protein levels in TSECs (Figure 2B). Co-culture of activated TSEC cells with freshly isolated neutrophils resulted in increased adhesion of the latter to the TSEC monolayers, indicating a correlation between *Sele* expression and neutrophil recruitment (Figure 2C and D).

Deletion of the Sele Gene Slightly But Significantly Reduces Liver Damage Associated With Simple Steatosis in HFD-Fed Mice

To examine the role of E-selectin in the pathogenesis of nonalcoholic fatty liver disease, we first used E-selectin KO mice (*Sele* KO) fed a HFD for 3 or 6 months, and found that after 3 months of HFD feeding, *Sele* KO showed a decreasing trend in serum levels of alanine aminotransferase (ALT) and aspartate aminotransferase (AST) compared with wild type (WT) mice (Figure 3A). This difference, however, was not statistically significant. Furthermore, no changes in characteristic liver steatosis, body weight, or liver to body weight ratio were observed between WT and *Sele* KO mice (Figure 3B and C). MPO staining also indicated no changes in neutrophil recruitment (Figure 3D). However, when HFD feeding was prolonged for 6 months, a small yet significant reduction of ALT and AST levels was found in the *Sele* KO cohort compared with WT mice (Figure 3E). This reduction in liver enzyme levels was in line with a decrease in liver weight and liver to body weight ratio (Figure 3F), suggesting a beneficial effect of knocking out E-selectin in steatosis-associated liver injury. Furthermore, serum glucose levels in HFD-fed *Sele* KO mice were significantly higher than those in WT animals (Figure 3G), which prompted the question of whether HFD-induced glucose metabolism could be different between *Sele* KO and WT mice. A glucose tolerance test (GTT) showed similar levels of insulin resistance in HFD-fed WT and *Sele* KO mice, compared with chow-fed WT mice (Figure 3H). However, the insulin tolerance test (ITT) showed that *Sele* KO mice had a higher insulin sensitivity than their WT counterparts, which might explain the slight reduction of body weight observed in *Sele* KO mice. It should be noted, however, that the small differences in liver enzyme levels, body weight, liver weight to body weight ratio, and glucose metabolism were only statistically significant when large animal cohorts (WT, n = 26; *Sele* KO, n = 31) were compared.

Deletion of the Sele Gene Reduces Liver Injury and Fibrosis in HFD^{+AdCxcl1}-Induced NASH by Decreasing Reactive Oxygen Species, p38, and c-Jun-N-Terminal Kinase Activation

Hepatocyte apoptosis represents one of the major pathogenic events responsible for the transition of steatosis to NASH²⁶ and was more significant in the HFD^{+AdCxcl1}-induced NASH model than in the HFD-induced steatosis model.⁶ Therefore, we investigated the effect of *Sele* KO on liver damage in the HFD^{+AdCxcl1} model. Under

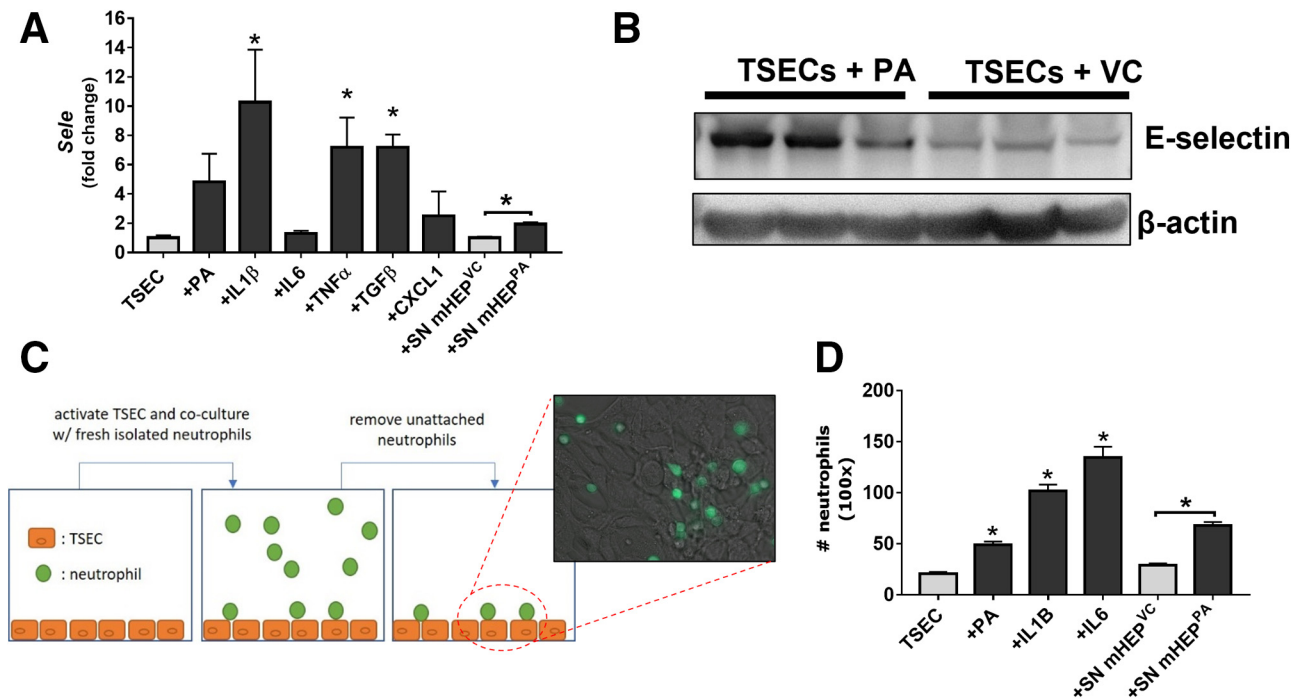


Figure 2. E-selectin expression in activated endothelial cells correlates with neutrophil adhesion. (A) RT-qPCR analysis of immortalized mouse endothelial cells (TSECs) exposed to inflammatory triggers or supernatant from primary hepatocytes exposed to palmitic acid (PA) or vehicle (VC) for 24 hours. (B) Western blot analyses of E-selectin protein in TSECs exposed to PA or VC for 24 hours. (C) Schematics of the co-culture of TSEC and enhanced green fluorescent protein (eGFP)-expressing neutrophils. (D) Quantification of eGFP-expressing neutrophils adhered to TSECs that are activated by various inflammatory mediators. * $P < .05$ compared with TSEC controls, # $P < .05$ compared with corresponding VC samples.

these conditions, *Sele* KO mice had significantly lower serum levels of ALT and AST than WT mice (Figure 4A), without differences in body weight or liver to body weight ratio (Figure 4B). This coincided with a reduction of MPO⁺ and F4/80⁺ cells in the liver (Figure 4C–E). Immunocytochemistry staining for ionized calcium binding adaptor molecule 1, which is a pan-macrophage marker, and C-type lectin domain family 4 member F, which marks only tissue-resident Kupffer cells,^{27,28} showed that the ratio between resident Kupffer cells and infiltrated macrophages is the same between WT and *Sele* KO mice (Figure 4F) although the total number of macrophages in the liver was reduced in *Sele* KO mice than in WT mice (Figure 4E). This suggests that the observed reduction in hepatic macrophages in *Sele* KO mice is owing to both a reduction in resident Kupffer cells and infiltrated macrophages. Furthermore, the reduction in hepatic neutrophils and macrophages was not caused by a disturbance in circulating cells because the number of white blood cells (neutrophils, monocytes, leukocytes, and lymphocytes) remained the same in both WT and *Sele* KO NASH mice (Figure 4G), confirming a specific role of E-selectin in NASH pathogenesis. The decrease in liver injury was supported further by a reduction in hepatic apoptosis indicated by terminal deoxynucleotidyl transferase-mediated deoxyuridine triphosphate nick-end labeling staining (Figure 5A) and determination of poly (adenosine diphosphate-ribose) polymerase in the liver (Figure 5B). The observed

decrease in death receptor 5 (*Dr5*), *Ly6g*, and *Adgre1* mRNA levels in *Sele* KO mice further supported the observed decrease in apoptosis and inflammatory cell infiltration (Figure 5C). In addition, hepatic levels of lipid peroxide 4-hydroxynonenal were lower in *Sele* KO mice than those in WT mice (Figure 5D and E), suggesting that hepatic oxidative stress is reduced in *Sele* KO mice. In agreement with these findings, hepatic activation of stress kinases such as p38 and c-Jun-N-terminal kinase (JNK) was lower in *Sele* KO mice when compared with WT mice, although the levels of apoptosis signal-regulating kinase 1 were comparable between *Sele* KO and WT controls (Figure 5E).

To further investigate whether E-selectin KO has persistent effects on the progression of NASH, we investigated the alterations in fibrosis and steatosis between *Sele* KO and WT mice treated with HFD+*Cxcl1*. Compared with WT mice, *Sele* KO mice had a strong reduction in Sirius Red staining of collagen fibers (Figure 6A), reduction in mRNA levels of fibrogenic genes, transforming growth factor β (*Tgfb*) and *Acta2* (Figure 6B), and a reduction of α -smooth muscle actin protein (Figure 6C). Determination of liver fat in WT and *Sele* KO mice under HFD+*Cxcl1* conditions did not show any difference between these 2 groups as illustrated by Oil Red O lipid staining (Figure 6D) and by quantitative determination of hepatic triglycerides (Figure 6E). Furthermore, RT-qPCR analysis showed that the expression of fatty acid translocase (*Cd36*), which

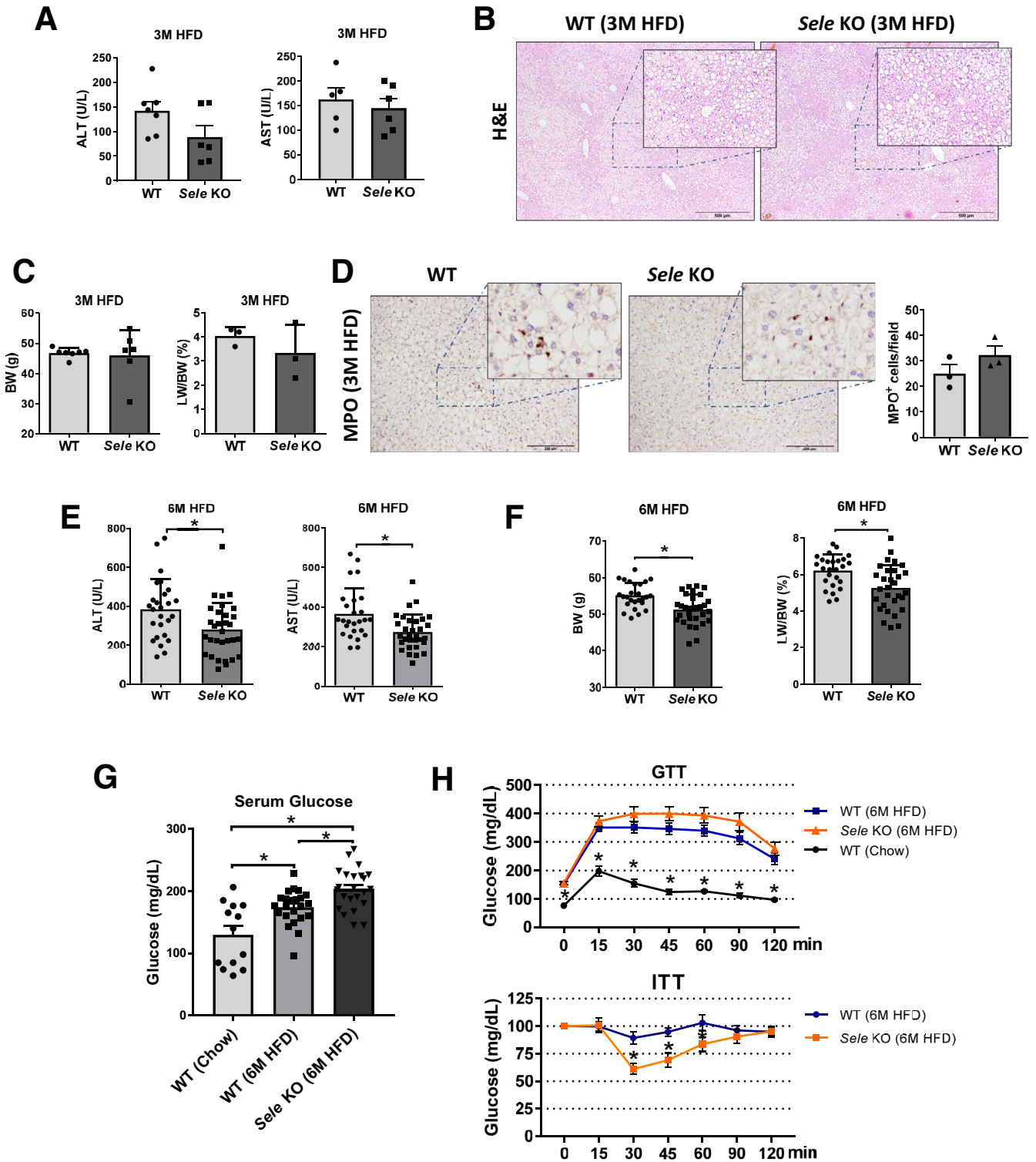


Figure 3. Deletion of the *Seleno* gene slightly reduces liver damage in HFD-fed mice. (A–D) WT (n = 7) and *Sele* KO (n = 6) mice were subjected to 3-month HFD feeding (3M HFD). (E and F) WT (n = 20–23) and *Sele* KO (n = 23) mice were subjected to 6-month HFD feeding (6M HFD) or chow diet (n = 13) (WT Chow). Sera and liver tissues were collected and analyzed. (A) Serum ALT and AST levels of 3M HFD. (B) H&E staining of liver tissue. (C) Body weight (BW) and liver weight to body weight ratio (LW/BW). (D) MPO immunostaining of liver tissues. (E) Serum ALT and AST levels. (F) BW and LW/BW. (G) Serum glucose levels and (H) GTT and ITT. **P* < .05.

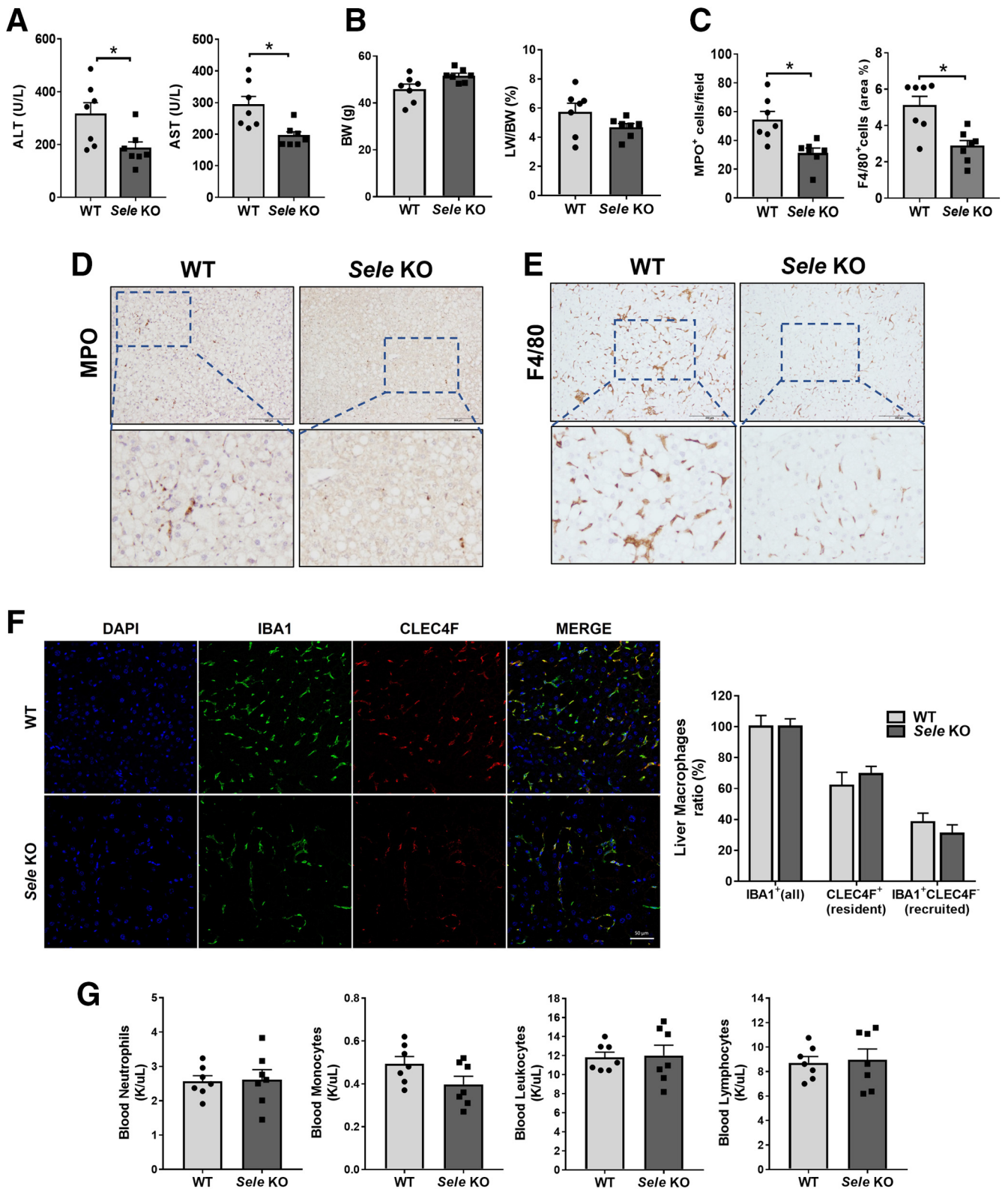


Figure 4. Deletion of the *Sele* gene ameliorates hepatocellular injury in HFD + AdCxcl1-induced NASH. WT (n = 7) and *Sele* KO (n = 6–7) mice were subjected to 3-month HFD feeding plus AdCxcl1 to induce NASH. Blood, sera, and liver tissues were collected and analyzed. (A) Serum ALT and AST levels. (B) Body weight (BW) and liver to body weight ratio (LW/BW). (C–E) MPO and F4/80 immunostaining of liver tissues. (F) Ionized calcium binding adaptor molecule 1 (IBA1) (all macrophages) and C-type lectin domain family 4 member F (CLEC4F) (resident Kupffer cells) immunofluorescence staining and cell ratio determination. (G) Blood leukocyte determination. *P < .05. DAPI, 4',6-diamidino-2-phenylindole.

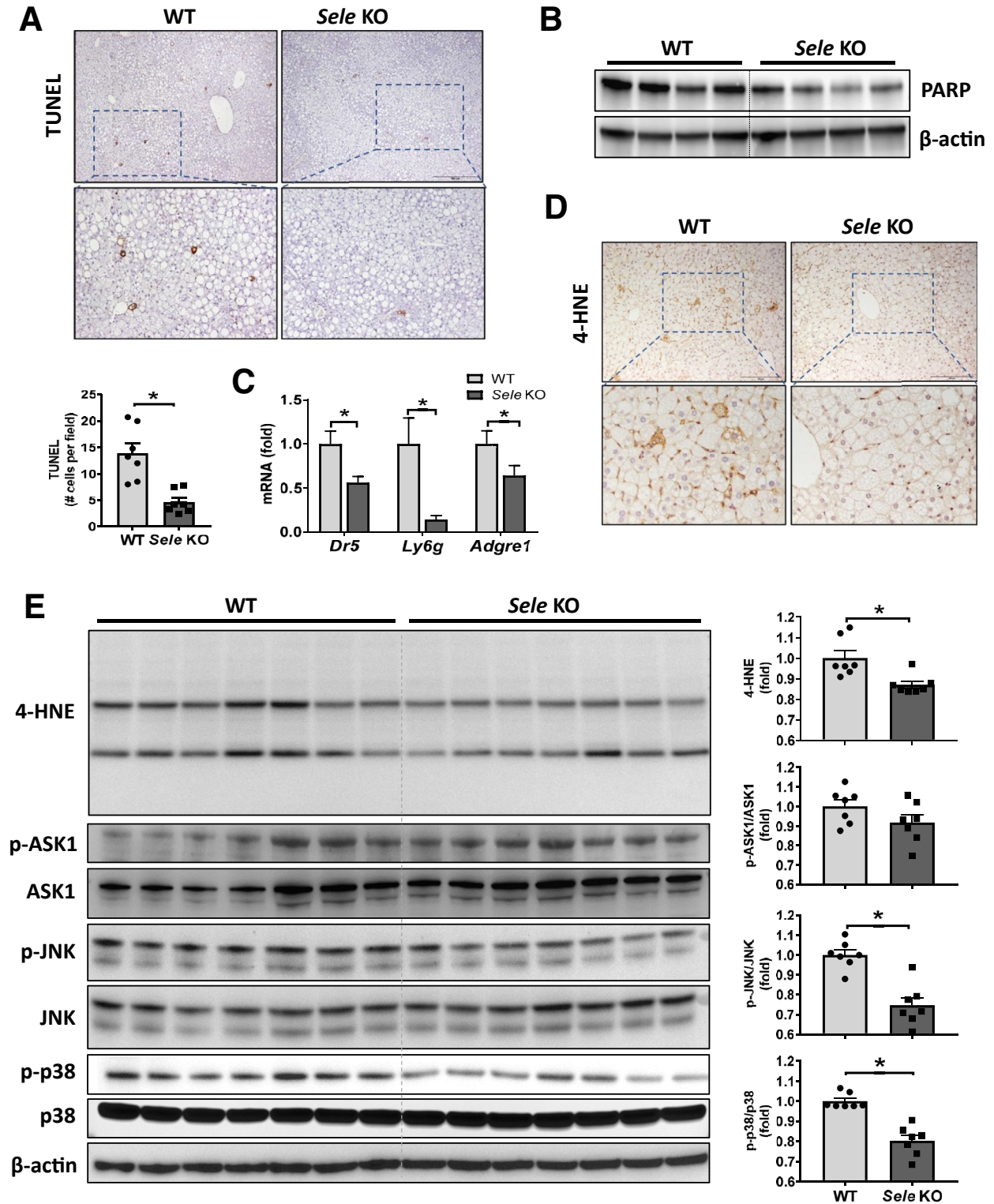


Figure 5. Deletion of the *Sele* gene decreases apoptosis, reactive oxygen species, p38, and c-Jun-N-terminal kinase (JNK) stress kinases in HFD + *AdCxc11*-induced NASH. WT (n = 7) and *Sele* KO (n = 6–7) were subjected to 3-month HFD feeding plus *AdCxc11* to induce NASH. Sera and liver tissues were collected and analyzed. (A) Terminal deoxynucleotidyl transferase-mediated deoxyuridine triphosphate nick-end labeling (TUNEL) staining of liver tissues. (B) Western blot determination of poly (adenosine diphosphate-ribose) polymerase (PARP) in liver tissues. (C) RT-qPCR of liver tissues. (D) 4-hydroxynonenal (4-HNE) staining of liver tissues. (E) Western blot analyses of liver tissues and quantification of protein densities. **P* < .05.

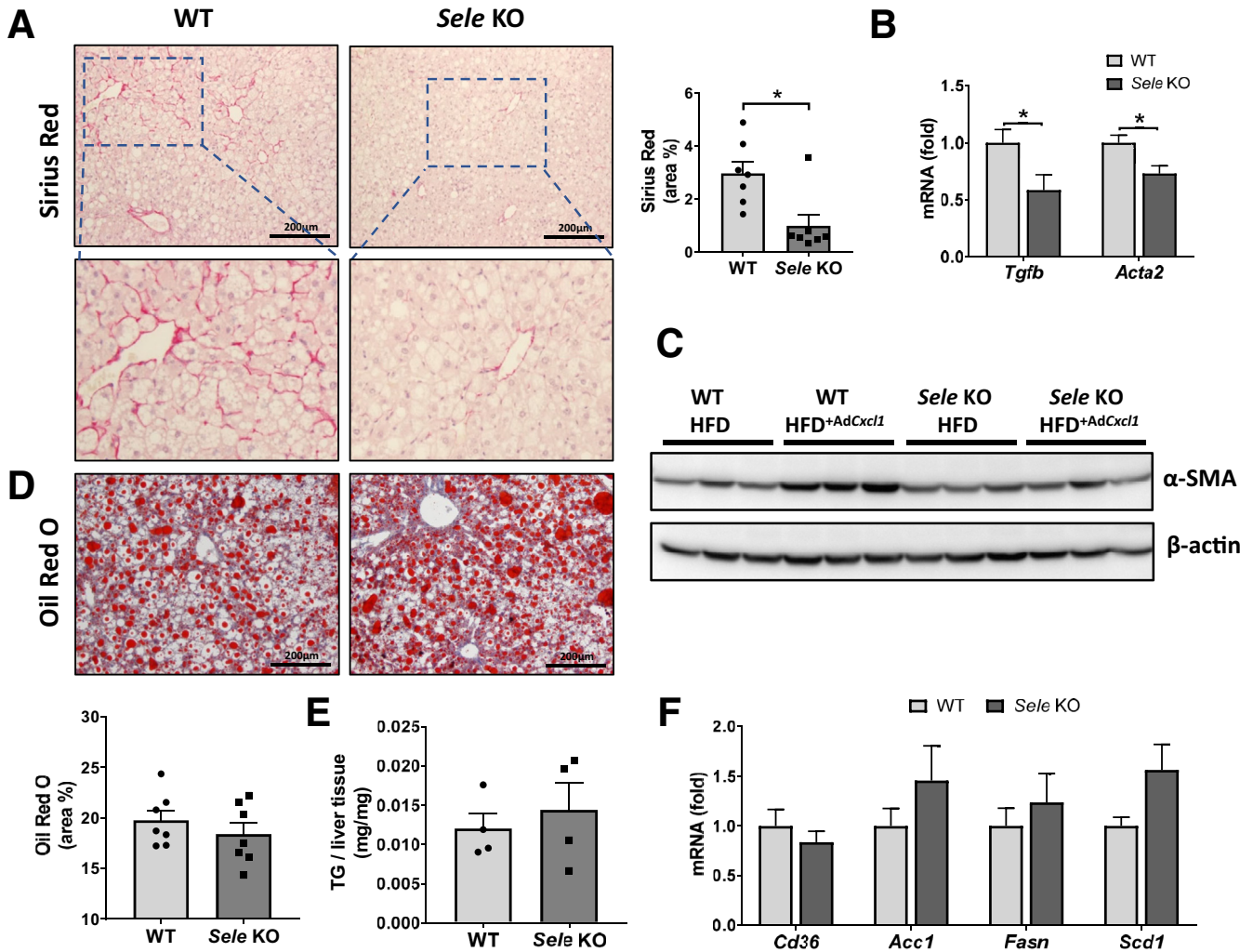


Figure 6. E-selectin KO reduces hepatic fibrosis but not steatosis in HFD^{+AdCxc11}-induced NASH. WT (n = 7) and *Sele* KO (n = 7) were subjected to 3-month HFD feeding plus *AdCxc11* to induce NASH. Liver tissues were collected and analyzed. (A) Sirius red staining of liver tissues. (B) RT-qPCR of liver tissues. (C) Western blot determination of α -smooth muscle actin (α -SMA) in liver tissues. In this panel, HFD feeding plus *AdGfp* (HFD) were used as controls. (D) Oil Red O staining of liver tissues. (E) Triglyceride (TG) determination of liver samples (n = 4). (F) RT-qPCR of liver tissues. **P* < .05.

functions as the main importer of fatty acids into hepatocytes²⁹ as well as de novo lipogenesis genes, did not differ between WT and *Sele* KO mice (Figure 6F).

We also tested the role of E-selectin in another model of NASH induced by feeding a Western diet for a 10-week period. The Western diet induced a typical steatotic phenotype and great liver injury in both WT and *Sele* KO mice (Figure 7A and B). Surprisingly, WT and *Sele* KO mice did not show any differences in ALT, AST, or liver MPO⁺ cells (Figure 7C and D). Although the Western diet (high-fat, high-cholesterol, and high-sucrose diet) often is suggested as a NASH-inducing diet, liver injury in this model may be caused mainly by high-cholesterol-induced hepatotoxicity and not by neutrophils, which may be why Western diet-induced liver injury was not reduced in *Sele* KO mice.

Deletion of the *Sele* Gene Lowers Inflammation, Lipolysis, and Adipokine Secretion in Adipose Tissue in HFD^{+AdCxc11}-Induced NASH

Adipose tissue inflammation generally has been associated with the severity of NAFLD.^{9,30} We previously showed that adipocyte death contributes to liver injury by promoting the release of FFA into circulation and inducing hepatic macrophage infiltration and activation.³¹ However, how immune cell infiltration in adipose tissue affects the progression of liver injury has not yet been documented. To understand this question, we evaluated the immune cell infiltration in adipose tissue of WT and *Sele* KO mice after HFD^{+AdCxc11} challenge. MPO and F4/80 immunostaining (Figure 8A) and RT-qPCR analyses of their corresponding genes (*Ly6g* and *Adgre1*) (Figure 8B)

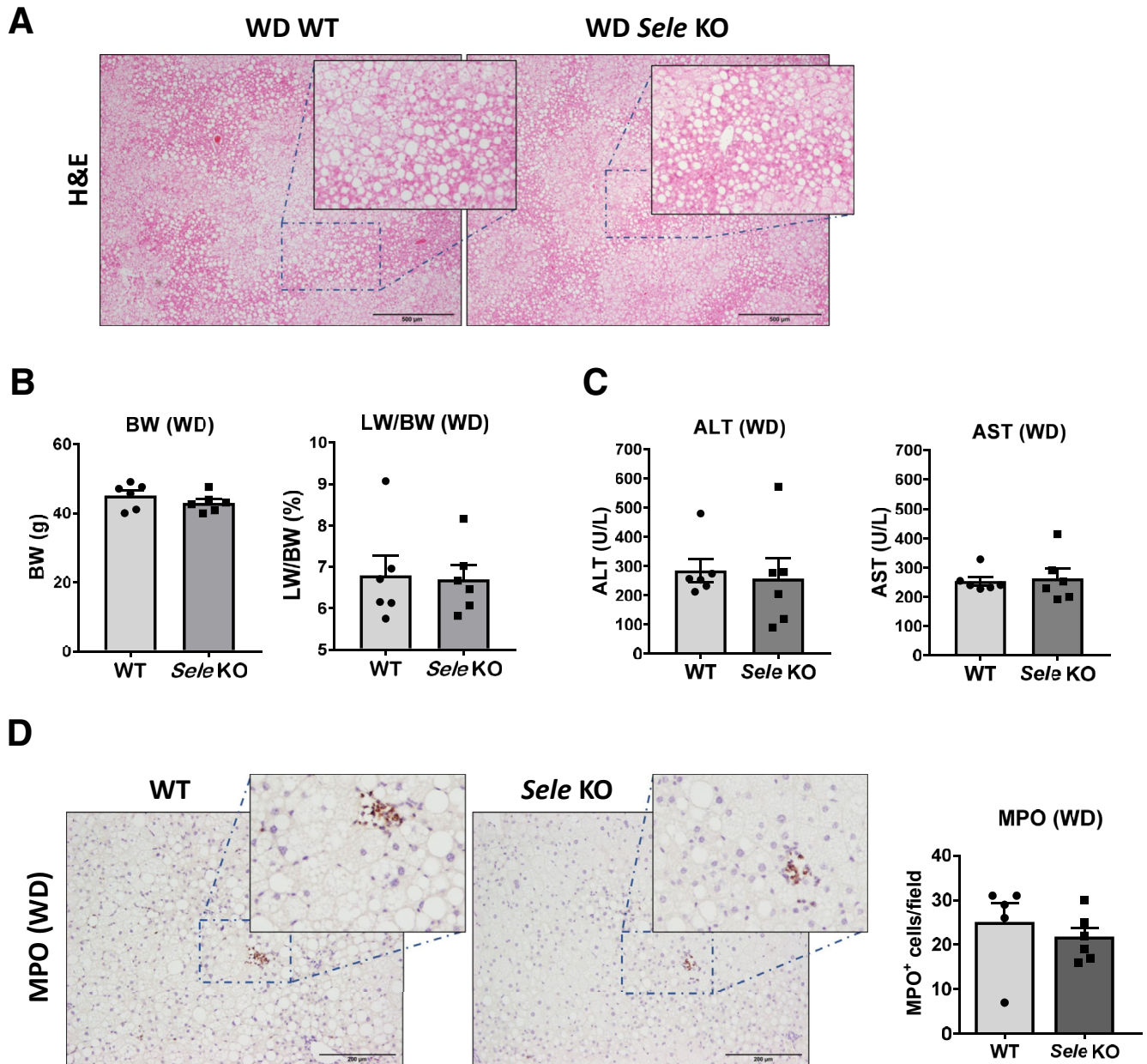


Figure 7. E-selectin KO does not reduce liver injury in Western diet (WD)-fed mice. WT ($n = 6$) and *Sele* KO ($n = 6$) mice were put on a WD for 10 weeks to induce NASH. Serum and liver samples were collected and analyzed. (A) H&E staining of liver tissues. (B) Body weight (BW) and liver weight to body weight (LW/BW) ratio. (C) Serum ALT and AST levels. (D) MPO immunostaining of liver tissues.

showed that compared with WT mice, *Sele* KO mice had a reduction of neutrophils and macrophages in epididymal adipose tissue, which correlated with a lower gene expression of E-selectin ligands *Cd44* and *Selplg* and of proinflammatory cytokines *Il1b*, *Ccl2*, and *Tnfa* (Figure 8B). Interestingly, the expression of lipolysis-related gene *Hsl* and *Atgl*³² also was reduced markedly in *Sele* KO mice (Figure 8C), which correlated with a reduction of serum FFA (Figure 8D).

There is increasing evidence that alterations in proinflammatory adipokines produced by adipose tissue play a role in adipose tissue inflammation and contribute to the development of NASH.^{21,33–35} Therefore, we investigated the expression patterns of multiple adipokines in adipose tissue and found that the expression of *Retn*, insulin-like growth factor-binding protein 1 (*Igfbp1*), leptin (*Lep*), retinol binding protein 4 (*Rbp4*), and S100 calcium-binding protein A8 (*S100a8*) and *S100a9* mRNA levels was reduced in *Sele*

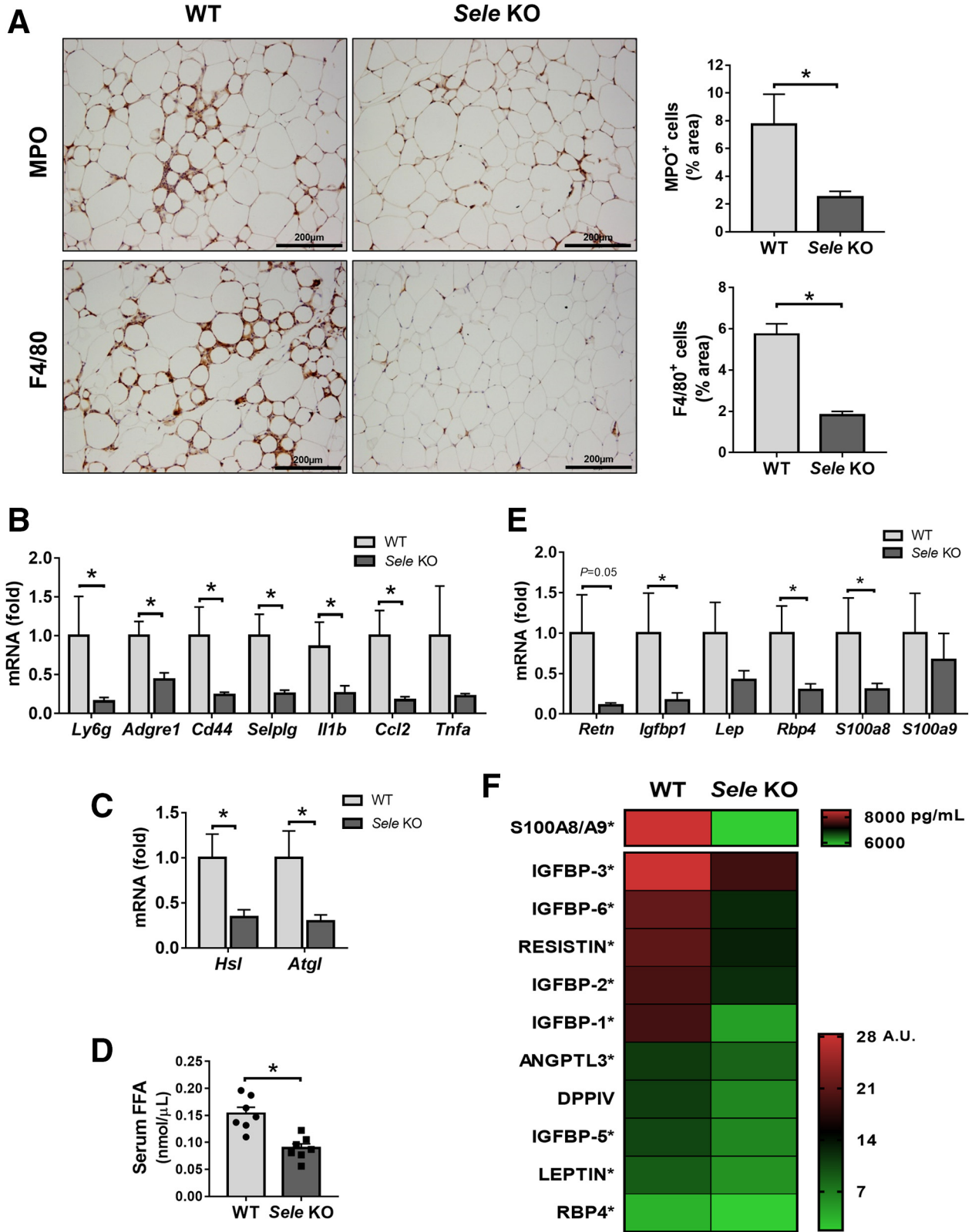


Figure 8. Genetic deletion of the *Sele* gene reduces inflammation, lipolysis, and proinflammatory adipokine secretion in adipose tissue from HFD + *AdCxl1*-induced NASH. WT (n = 4–7) and *Sele* KO (n = 4–7) were subjected to 3-month HFD feeding plus *AdCxl1* to induce NASH. Sera and epididymal adipose tissues were collected and analyzed. (A) MPO and F4/80 immunostaining of adipose tissues. (B, C, and E) RT-qPCR of adipose tissues. (D) Determination of serum FFAs. (F) Determination of serum proinflammatory adipokines. **P* < .05.

KO mice compared with WT controls under the HFD^{+AdCxcl1} challenge (Figure 8E). In addition, we investigated the serum protein levels of multiple adipokines and found that several proteins, including the S100A8/A9 dimer, multiple members of the IGF1 family, resistin, angiopoietin-like protein 3 (ANGPTL3), dipeptidyl peptidase 4, leptin, and RBP4, were present at lower levels in *Sele* KO mice compared with WT mice (Figure 8F).

E-Selectin-Dependent S100A8/A9 Expression Is Up-regulated in Adipose Tissue During NASH

The earlier-described data suggest that reduction of neutrophil and macrophage recruitment in adipose tissue via deletion of *Sele* lessens the NASH phenotype by reducing tissue inflammation and lipolysis. To understand the mechanism by which neutrophils in adipose tissue exacerbate steatosis-to-NASH progression, we focused on neutrophil-enriched proteins S100A8 and S100A9, which were reduced markedly in adipose tissue and serum from *Sele* KO mice compared with WT mice as described earlier. We first analyzed transcriptomic data sets of adipose tissue⁹ from patients and found a significant up-regulation of *S100A8* and *S100A9* in the adipose tissue samples of NASH patients, compared with tissue of patients with normal livers (Figure 9A). Inversely, the expression of these genes in the liver was down-regulated in NASH patients compared with patients with steatosis or normal liver (Figure 9B) based on analysis of transcriptomic data sets of NASH liver samples.²⁵

The role of S100A8/A9 was investigated further using the HFD^{+AdCxcl1}-induced NASH model. Western blot analysis and histochemical staining of adipose tissue of mice under HFD^{+AdCxcl1} conditions showed much higher S100A8/A9 levels compared with HFD-fed mice (Figure 9C), supporting the clinical data in Figure 9A. However, this induction was much less evident in the liver (Figure 9D). Immunohistochemistry analyses showed that strong S100A8/A9 protein staining was observed in adipose tissue of WT mice under HFD^{+AdCxcl1} conditions and such staining was diminished markedly in *Sele* KO mice (Figure 9E and F). Surprisingly, the liver tissues from HFD^{+AdCxcl1}-treated WT mice only had weak S100A8/A9 protein staining, which was slightly reduced in *Sele* KO mice (Figure 9E). Finally, Western blot analyses also showed strong expression of S100A8/A9 protein in adipose tissue but weak expression in liver tissues, with reduced levels in *Sele* KO mice compared with WT mice (Figure 9G).

S100A9 Inhibitor Ameliorates NASH in Mice via Inhibition of Lipolysis in Adipose Tissue

To examine the roles of S100A8/A9 in neutrophil-driven NASH, we treated HFD^{+AdCxcl1}-challenged mice with the S100A9 inhibitor PAQ (schematic in Figure 10A). Administration of 10 or 20 $\mu\text{g}/\text{kg}$ PAQ markedly reduced serum ALT and AST levels (Figure 10B) without affecting body weight or liver to body weight ratio (data not shown). This reduction in liver injury correlated with a decreasing trend in mRNA levels of the apoptotic marker *Dr5* and a significant reduction of inflammatory markers *Il1b*, *Ccl2*, *Ifng*, and

Tnfa. Moreover, *Adgre1* and *Ly6g* mRNA levels, which encode macrophage F4/80 and neutrophil lymphocyte antigen 6 complex locus G6D marker proteins, respectively, remained unchanged (Figure 10C), indicating that the amount of these cells in the liver was not affected by the treatment. In addition, hepatic expression levels of fibrogenic genes including *Acta2*, *Col1a1*, *Col1a2*, *Col3a1*, and *Col4a1* also were ameliorated when the highest concentration of PAQ was administered (Figure 10D). In adipose tissue, expression of the apoptotic and inflammatory markers was reduced after administration of PAQ, but this reduction did not reach statistical significance (Figure 10E). Interestingly, the expression of lipolysis-related genes including *Hsl*, *Atgl*, and *Plin1* in adipose tissue was reduced markedly in the 20 $\mu\text{g}/\text{kg}$ PAQ group (Figure 10F). Such reduction in lipolysis-related genes correlated with a significant decrease in serum FFA (Figure 10G). Furthermore, a trend in reduction of adipokine mRNA levels also was observed, although these differences were not statistically significant (Figure 10F). However, treatment with 10 $\mu\text{g}/\text{kg}$ PAQ significantly reduced the serum levels of resistin (Figure 10H).

To further pinpoint the effect of S100A8/A9 in adipose tissue, we exposed differentiated adipocytes to a recombinant mouse S100A8/A9 dimer in vitro and found that such treatment markedly up-regulated lipolysis-related gene expression, as indicated by a significant increase of *Hsl* and *Atgl* (Figure 10I). Exposure to S100A8/A9 also significantly up-regulated *Retn* and showed an increasing trend in *Lep* and *Rbp4* expression in adipocytes in vitro.

Discussion

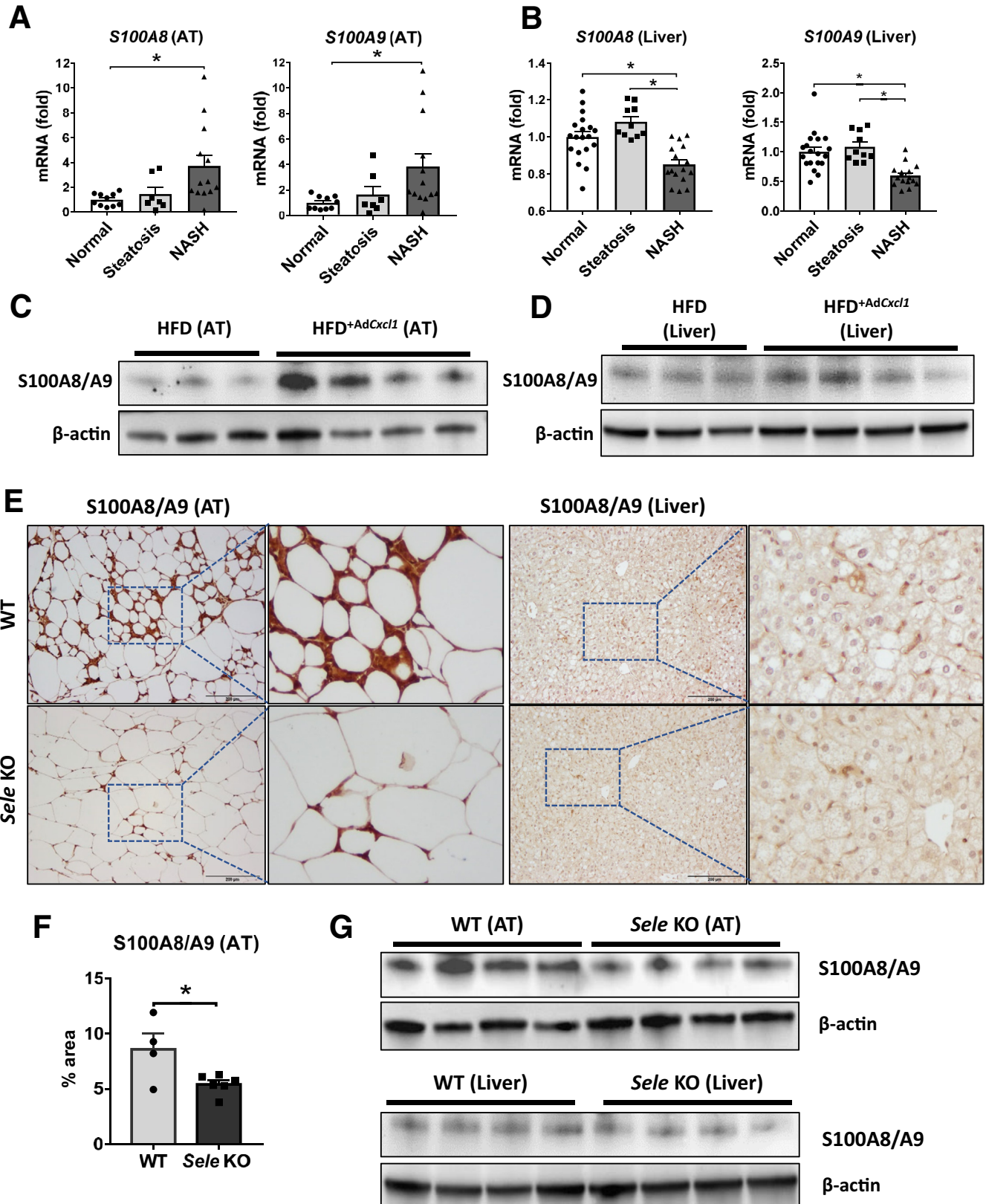
The risk for adverse outcomes in patients with simple steatosis is low, but can increase rapidly when this condition evolves to NASH.³⁶ The exact mechanisms that drive this steatosis-to-NASH progression are still not fully elucidated, however, triggers of liver inflammation can have their origins in the liver itself or in another organ such as adipose tissue or the gut.³⁷ We have shown previously that overexpression of the neutrophil chemokine CXCL1 causes neutrophil infiltration and NASH in HFD-fed mice by producing reactive oxygen species and activating the stress kinase p38.^{6,38} However, exactly how neutrophils in adipose tissue affect the development and progression of NASH has not been documented.

In the current study we uncovered that the expression of E-selectin, which plays a crucial role in the initial stages of neutrophil recruitment,¹⁰ is increased during NASH at markedly higher levels in adipose tissue than in the liver, suggesting that E-selectin-dependent inflammation occurs predominantly in adipose tissue. Our data further showed that several inflammatory cytokines and FFAs were able to up-regulate E-selectin in endothelial cells. It is known that adipose tissue likely has higher levels of FFAs than liver tissue, which probably contributes, at least in part, to the greater induction of E-selectin in adipose tissue when compared with liver tissue.

E-selectin was documented previously to be implicated in inflammation of the liver^{14,39} and adipose tissue.⁴⁰

Increased soluble E-selectin in plasma has been shown to be associated with NAFLD severity in patients.^{39,41} However, how E-selectin contributes to the NAFLD pathogenesis

remains unknown. Now, we provide evidence supporting that this molecule indeed plays a specific regulating function during the steatosis-to-NASH transition. First, E-selectin



induction in adipose tissue or the liver was observed during HFD^{+AdCxcl1}-induced NASH but not simple steatosis, hinting at a NASH-specific function of this adhesion molecule. Second, genetic deletion of the *Sele* gene resulted in a significant decrease in liver injury in HFD^{+AdCxcl1}-induced NASH, as indicated by a decrease in serum aminotransferase levels and liver apoptosis, which corroborated with reduced activation of p38 and JNK stress kinases. Third, decreased liver fibrosis in *Sele* KO mice further substantiated a reduction in NASH phenotype associated with E-selectin loss of function. Interestingly, the effect of E-selectin ablation overrides the effect of CXCL1 in inducing neutrophil infiltration in the liver. We speculate that the chemoattractant action of CXCL1 induces the transport of neutrophils to the liver, but that the adhesion of these cells to sinusoidal endothelial cells is compromised in the *Sele* KO mice and, as a result, the cells that remain in circulation are removed by the blood flow.

E-selectin KO also showed a reduction in serum aminotransferase levels on a HFD-induced steatosis mouse model. However, this reduction was observed only when the period of HFD was prolonged (6 months instead of 3 months), and was only statistically significant when a high number of mice in each group was used. Because prolonged HFD feeding has been associated with an increase of inflammation and progression of NAFLD,⁴² it is reasonable to assume that these 6-month HFD-fed mice already have a more advanced form of NAFLD in which more inflammation is present and therefore the role of E-selectin becomes more prominent.

As per the leukocyte adhesion cascade paradigm, a coordinated sequential action of several adhesion molecules is required for the recruitment of circulating leukocytes to areas of inflammation.¹⁰ Therefore, besides E-selectin, other adhesion molecules also may play a role in steatosis-to-NASH progression. It recently was documented that hepatic mRNA levels of L-selectin, which is expressed on most types of lymphocytes, but particularly on neutrophils,^{43,44} was induced in patients with steatosis and increased further in patients with NASH.⁴⁵ The same study also reported that deletion or therapeutic blockade of L-selectin prevented the development and progression of steatohepatitis in HFD- and MCD-diet-fed mice. In our study, we found that the modulation of *SELL* expression in patients with NASH was markedly lower than that of *SELE*, which also was more specific to the NASH condition because no induction was observed in steatosis samples compared with normal livers. Thus, we surmise that E-selectin plays a more specific role than L-selectin in steatosis-to-NASH progression.

Similar to the liver, a clear reduction of inflammation also was observed in adipose tissue of *Sele* KO mice during HFD^{+AdCxcl1}-induced NASH. Compared with WT mice, *Sele* KO mice had a decrease in infiltration of neutrophils and macrophages, and a reduction in the expression and secretion of proinflammatory adipokines such as IGFBP, resistin, leptin, RBP4, and ANGPTL3 in adipose tissue. These changes probably contribute to the improved NASH phenotypes in *Sele* KO mice because increased serum values of resistin, leptin, RBP4, and ANGPTL3 have been suggested to promote NASH pathogenesis,^{33,46} and an increase of IGFBPs was associated with advanced fibrosis.^{47,48} Moreover, we found that S100A8/A9 was highly induced in adipose tissue of mice under NASH conditions and markedly reduced if *Sele* KO mice were used. These observations were much less prominent in the liver, substantiating the differences in E-selectin expression between adipose tissue and the liver and the consequential difference in S100A8/A9 levels in these tissues. S100A8 and S100A9 proteins are unstable and therefore most often exist in the form of a stable S100A8/A9 heterodimer, which comprises approximately 45% of the cytoplasmic proteins in neutrophils.⁴⁹ S100A8/A9 has been documented to stimulate leukocyte recruitment and induce cytokine secretion.¹⁵ In the current study, we showed that S100A8/9 plays an important role in promoting NASH as treatment with the S100A8/9 inhibitor PAQ considerably improved the NASH phenotype.

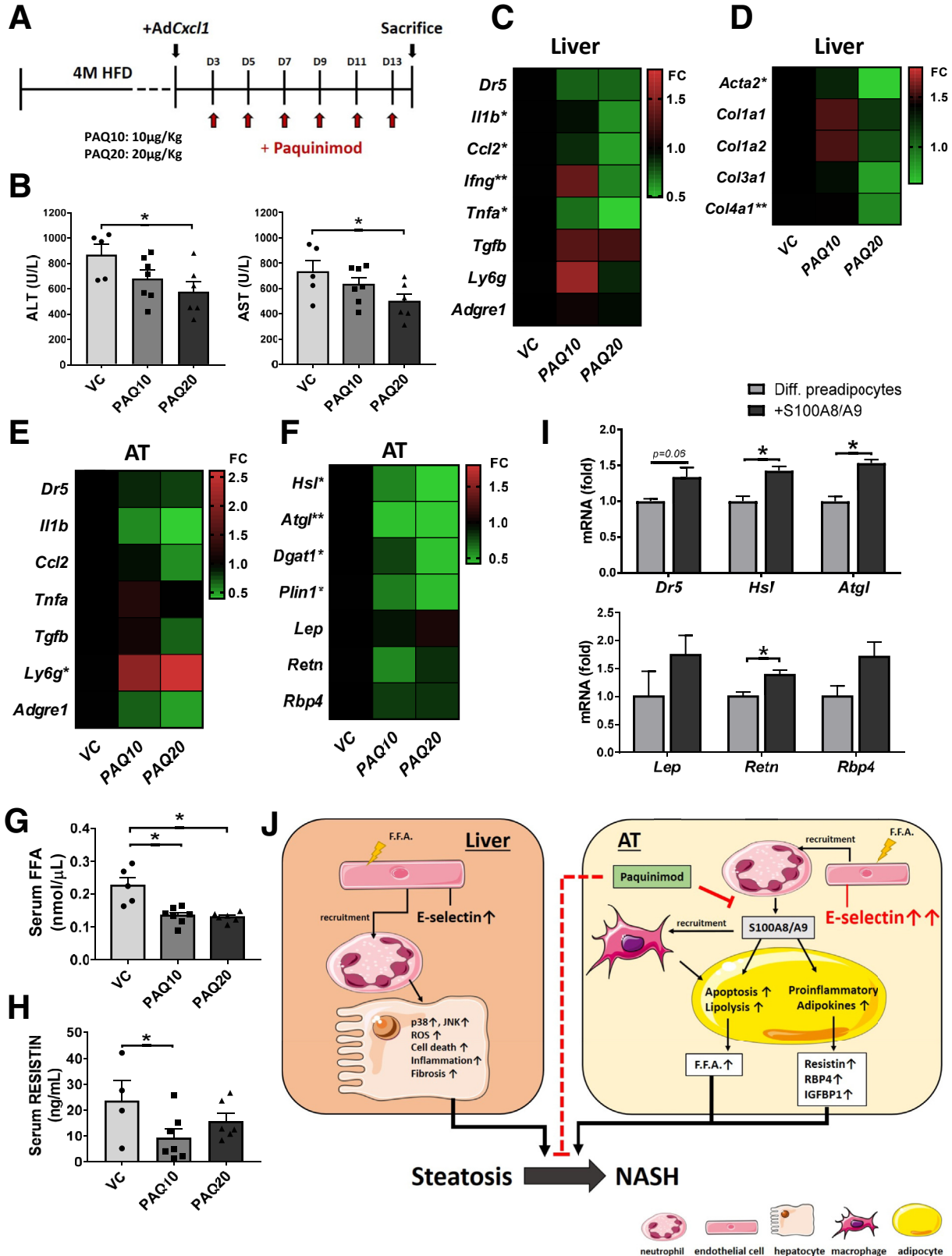
Another important observation from the current study was the striking reduction of lipolysis-related genes in adipose tissue of *Sele* KO mice during HFD^{+AdCxcl1}-induced NASH, which resulted in a decrease in secretion of FFA and proinflammatory adipokines that are known to promote liver injury.^{34,50} Increased FFA levels in the blood are known to directly induce hepatotoxicity and contribute to NASH pathogenesis.^{51,52} Therefore, our data suggest that E-selectin plays an important role in inducing lipolysis in adipose tissue and increasing circulating FFAs during NASH, contributing to NASH pathogenesis. The role of E-selectin in inducing lipolysis probably is mediated via the neutrophil recruitment and subsequent production of S100A8/A9 because inhibition of S100A8/A9 down-regulated lipolysis-related gene expression in adipose tissue, while treatment with S100A8/A9 protein up-regulated expression of these genes in cultured adipocytes.

Altogether, our data indicate that E-selectin-dependent neutrophil recruitment in both the liver and adipose tissue is an important driver of steatosis-to-NASH progression (Figure 10). E-selectin, however, triggers distinct pathogenic processes in the liver and in adipose tissue that

Figure 9. (See previous page). S100A8/A9 is up-regulated in adipose tissue but not in the liver during NASH, which is dependent on E-selectin. (A and B) Normalized gene expression (microarray data sets obtained from Du Plessis et al⁹ and Lake et al²⁵) in visceral adipose tissue (AT) and liver of patients suffering from steatosis ($n_{AT} = 7$, $n_L = 10$) and NASH ($n_{AT} = 13$, $n_L = 16$) compared with healthy controls (normal) ($n_L = 19$, $n_{AT} = 8$). (C and D) WT mice were subjected to 3-month HFD plus AdCxcl1 (HFD^{+AdCxcl1}) to induce NASH or HFD+AdGfp (HFD) as controls. Adipose and liver tissues were collected and analyzed. Western blot analyses of S100A8/A9 dimer in adipose and liver tissues. (E–G) WT and *Sele* KO were subjected to 3-month HFD plus AdCxcl1 to induce NASH. Adipose and liver tissues were collected and analyzed. (E, left; and F) Immunostaining analyses of S100A8/A9 in adipose tissue and (E, right) liver tissues. (G) Western blot analyses of S100A8/A9 dimer of adipose tissues (top panel) and liver tissues (bottom panel). * $P < .05$.

together exacerbate the steatosis-to-NASH progression. Although it is difficult to weigh the detrimental effect of E-selectin in each organ, we speculate that it plays a more prominent role in adipose tissue because E-selectin

expression is increased during NASH at markedly higher levels in adipose tissue compared with the liver. Targeting E-selectin-induced adipose tissue inflammation therefore may represent a potential novel therapy for treatment of NASH.



Material and Methods

Animal Experiments

All animal experiments were approved by the National Institute on Alcohol Abuse and Alcoholism's Animal Care and Use Committee and conducted in accordance with National Institutes of Health guidelines. C57BL/6J and B6.129S4-*Sele*^{tm1Dmil}/J (*Sele* KO) mice originally were obtained from The Jackson Laboratory (Bar Harbor, ME) and further bred at the National Institute on Alcohol Abuse and Alcoholism animal facility.

HFD^{+AdCxcl1}-Induced Mouse Model of NASH

To generate CXCL1-induced NASH, 10- to 12-week-old male mice were fed an HFD (60 kcal% fat, D12492; Research Diets, New Brunswick, NJ) for 3 or 4 months and injected via tail vein with adenovirus-*Cxcl1* (Applied Biological Materials, Richmond, Canada). The mice then were kept on a HFD for 2 additional weeks after *AdCxcl1* injection before killing for analysis. The control mice were fed an HFD and received a tail vein injection of *AdGfp* instead of *AdCxcl1*. Paquinimod (Novus Biologicals, Centennial, CO) treatment was administered at 2 different doses, namely 10 and 20 $\mu\text{g}/\text{kg}$, by intraperitoneal injection every second day starting 2 days after *AdCxcl1* injection. The mice were kept on a HFD during the treatment period and were killed 2 weeks after *AdCxcl1* infection.

Western Diet

To generate diet-induced steatohepatitis, 10- to 12-week-old C57BL/6J male mice were put on an Amylin Liver NASH D09100301 diet (40 kcal% fat, 20 kcal% fructose, 2% cholesterol; Research Diets), mimicking a Western diet, for 10 weeks. Mice fed a chow diet (10 kcal% fat) were used as controls.

Serum ALT and AST

Serum ALT and AST levels were determined using the Catalyst Dx Chemistry Analyzer (IDEXX Laboratories, Westbrook, ME) or ALT Kinetic and AST Kinetic (Teco Diagnostics, Anaheim, CA) according to the manufacturer's instructions.

Serum FFAs

Serum FFAs levels were determined using the Free Fatty Acid Quantification Colorimetric/Fluorometric Kit (BioVision, Milpitas, CA) according to the manufacturer's instructions.

Serum Glucose, GTT, and ITT

Serum glucose was measured using a glucometer (Bayer Corporation, St. Louis, MO). For the GTT and the ITT, mice were fasted for 16 hours or 4 hours, respectively, and allowed free access to water. Glucose (2 g/kg; Sigma Aldrich, St. Louis, MO) and insulin (1 U/kg, Humalog; Lilly, Indianapolis, IN) were injected intraperitoneally, respectively. Tail blood glucose levels were measured at 0, 15, 30, 45, 60, 90, and 120 minutes after glucose or insulin injection.

Serum Cytokines, Chemokines, and Adipokines

Serum levels of mouse CXCL1 were determined using the Mouse CXCL1/KC Quantikine enzyme-linked immunosorbent assay (ELISA) kit and serum levels of mouse S100A8/A9 were quantified using the Mouse S100A8/S100A9 Heterodimer DuoSet ELISA (both from R&D Systems, Minneapolis, MN) following the manufacturer's instructions. Resistin serum levels of were measured using the RayBio Mouse Resistin ELISA Kit (RayBiotech, Peachtree Corners, GA). The Proteome Profiler Mouse Adipokine Array Kit (R&D Systems) was used for the determination of IGF1, resistin, ANGPTL3, dipeptidyl peptidase 4, leptin, and RBP4 in serum samples pooled per group. The assay was repeated to generate a total of 4 measurements per group.

Blood Leukocyte Determination

A complete blood count test for blood leukocyte determination was performed on anticoagulated blood using a Hemavet 950 FS Hematology Analyzer (Drew Scientific, Dallas, TX).

Liver Triglyceride Determination

Approximately 50 mg of the frozen liver tissues were used for determination of triglyceride content with the Triglyceride Colorimetric Assay Kit (Cayman Chemical, Ann Arbor, MI), according to the manufacturer's instructions.

Immunohistochemistry and Immunofluorescence Staining

Mouse epididymal adipose tissue and liver samples were collected and fixed in formalin, unless otherwise specified. Paraffin sections (4- μm thick) were cut and deparaffinized for histologic analysis. H&E staining (Richard-Allan Scientific, Kalamazoo, MI), Sirius Red staining (Sigma), and terminal deoxynucleotidyl transferase-mediated deoxyuridine triphosphate nick-end labeling staining (ApoTag Peroxidase *In Situ* Apoptosis Detection Kit; Millipore, Burlington, MA) were performed according to the manufacturers'

Figure 10. (See previous page). Inhibition of S100A9 ameliorates liver damage and inflammation in NASH by lowering lipolysis and adipokines in adipose tissue. WT mice were subjected to 4-month HFD feeding, followed by injection of *AdCxcl1* and treatment with 2 different doses of PAQ: 10 $\mu\text{g}/\text{kg}$ (PAQ10) ($n = 7$) or 20 $\mu\text{g}/\text{kg}$ (PAQ20) ($n = 6$), or vehicle control (VC) ($n = 5$). Serum, liver, and adipose tissues were collected and analyzed. (A) Schematics for the administration of PAQ to HFD^{+AdCxcl1}-challenged mice. (B) Serum ALT and AST levels. (C and D) RT-qPCR of liver tissues. (E and F) RT-qPCR of adipose tissues. (G and H) Determination of serum FFAs and serum resistin. (I) RT-qPCR analyses of differentiated preadipocytes exposed to vehicle control or S100A8/A9. (J) Schematic illustration of the proposed role of E-selectin and S100A8/A9 in the liver and adipose tissue during neutrophil-induced NASH. * $P < .05$.

instructions. For immunohistochemistry, heat-induced epitope retrieval was performed in 3% citrate buffer followed by incubation of the paraffin-embedded sections in 3% H₂O₂. Blocking of nonspecific binding was performed using 3% normal goat serum for 10–60 minutes. The sections then were incubated with primary antibodies (Table 1) overnight at 4°C and subsequently with anti-mouse or anti-rabbit secondary antibodies (SignalStain Boost Immunohistochemistry Detection Reagent; Cell Signaling Technology, Danvers, MA) for 1 hour at room temperature. The staining was visualized using the Vectastain Elite ABC Staining Kit and 3,3'-diaminobenzidine tetra hydrochloride Peroxidase Substrate Kit (Vector Laboratories, Burlingame, CA) according to the manufacturers' instructions. Nuclear staining then was performed using hematoxylin (Richard-Allan Scientific), upon which the slides were dehydrated and mounted with Fisher Chemical Permount Mounting (Thermo Fisher Scientific, Waltham, MA). For immunofluorescence staining, after primary antibody incubation overnight, samples were incubated with secondary antibodies (goat anti-rabbit IgG, Alexa Fluor 488; streptavidin, Alexa Fluor 555 conjugate; Thermo Fisher Scientific) for 1 hour at room temperature. Nuclear staining was obtained by incubation with 1 mg/mL 4',6-diamidino-2-phenylindole for 5 minutes. Images were acquired using either a BX41 microscope for bright field images (Olympus, Bethlehem, PA) or a LSM 710 confocal microscope (Zeiss, Thornwood, NY) for fluorescent images.

Western Blot

Liver and adipose tissues were homogenized in RIPA buffer containing a cocktail of protease inhibitors (Santa

Cruz Biotechnology, Dallas, TX) according to the manufacturer's instructions. Protein extracts were quantified using the Pierce BCA Protein Assay Kit (Thermo Fisher) and adjusted with RIPA before loading onto 4%–12% Bis-Tris protein gels (Bio-Rad, Hercules, CA) and transferred to nitrocellulose membranes (Thermo Fisher). Primary antibodies used in the Western blots can be found in Table 1. Secondary horseradish-peroxidase-conjugated antibodies (Santa Cruz Biotechnology) were used. Protein bands were visualized with SuperSignal West Femto Maximum Sensitivity Substrate (Thermo Fisher).

Oil Red O Staining

Liver samples were snap-frozen in liquid nitrogen after killing and embedded in Tissue-Plus OCT Compound (Thermo Fisher Scientific) for cryosectioning. Cryosections (5- μ m thick) were washed with 60% isopropanol for 1 minute and stained with 0.6% Oil Red O solution (Sigma-Aldrich) for 30 minutes. After washing with 60% isopropanol and distilled water (3 times each), the nuclei were counterstained with hematoxylin and the slides were mounted for microscopy.

RT-qPCR

Total RNA was purified from snap-frozen adipose tissue, liver tissues, or cell cultures using TRIzol Reagent (Thermo Fisher) and Qiagen RNEasy Mini kit protocol (Qiagen, Valencia, CA) according to the manufacturer's instructions. Reverse transcription of RNA into complementary DNA was performed using the High-Capacity Complementary DNA Reverse Transcription kit (Thermo

Table 1. Antibodies

Primary antibody	Dilution	Source
4-HNE (mouse)	1:400 (staining) 1:1000 (WB)	Genox, Baltimore, MD
ASK1 (rabbit)	1:1000	Thermo Fisher
p-ASK1 (Thr838) (rabbit)	1:5000	Thermo Fisher
CD31 (rabbit)	1:200	Cell Signaling Technologies
CLEC4F (rat)	1:100	R&D Systems
E-selectin (biotinylated)	1:200 (staining) 1:5000 (WB)	R&D Systems
F4/80 (rabbit)	1:400	Cell Signaling Technology
IBA1 (rabbit)	1:1000	Avantor/VWR, Philadelphia, PA
JNK (rabbit)	1:1000	Cell Signaling Technology
p-JNK (Thr183/Tyr185) (rabbit)	1:1000	Cell Signaling Technology
MPO (rabbit)	1:1	Biocare Medical, Concord, CA
p38 (rabbit)	1:1000	Cell Signaling Technology
p-p38 (Thr180/Tyr182) (rabbit)	1:1000	Cell Signaling Technology
S100A8/A9 (mouse)	1:500 (staining) 1:5000 (WB)	Novus Biologicals
α -SMA (mouse)	1:5000	Sigma-Aldrich
β -actin (mouse)	1:5000	Abcam, Cambridge, MA

4-HNE, 4-hydroxynonenal; ASK1, apoptosis signal-regulating kinase 1; α -SMA, α -smooth muscle actin; CLEC4F, C-type lectin domain family 4 member F; IBA1, ionized calcium binding adaptor molecule 1; JNK, c-Jun-N-terminal kinase; p-ASK1, α -phosphorylated ASK1; p-JNK, phosphorylated JNK; p-p38, phosphorylated p38 kinase; WB, Western blot.

Fisher). Real-time PCR was performed using an ABI7500 RT-PCR system (Applied Biosystems, Foster City, CA). *18s*, *Gapdh*, *Actb*, and *Apob* were used as normalizing house-keeping genes. All primers used for RT-qPCR are listed in Table 2.

Isolation and Culture of Mouse Primary Hepatocytes

Mice were anesthetized with 30 mg/kg pentobarbital sodium intraperitoneally. The portal vein was cannulated, and the liver was perfused with ethylene glycol tetra-acetic acid and subsequently with 0.075% collagenase (Worthington, Lakewood, NJ) solution. The obtained mixture then was incubated on a shaker at 100 rpm for 10 minutes at 37°C. After the digestion the cell suspension was filtered through a 70- μ L nylon mesh and primary hepatocytes were collected after centrifugation at $50 \times g$ for 5 minutes. Hepatocytes were plated on cell culture recipients coated with Rat Tail Collagen Type I (Corning, Corning, NY) at a density of $\pm 50,000$ cells/cm² and further cultures in cell culture

medium composed of Dulbecco's modified Eagle medium, 10% fetal bovine serum, and penicillin-streptomycin (all from Thermo Fisher Scientific). After 4 hours, culture media were replaced to remove nonadhered cells and debris. The cells then were exposed to palmitic acid (600 μ mol/L) (Sigma) or vehicle control for 24 hours. Hereafter, the cell culture medium was removed, and the cells were cultured for a further 24 hours with fresh culture medium, which then was reconditioned to be used in TSEC experiments.

Isolation of Neutrophils

Bone marrow of C57BL/6-Tg(CAG-EGFP)10sb/J mice (The Jackson Laboratory), which have widespread enhanced green fluorescent protein (eGFP) fluorescence, with the exception of erythrocytes and hair, was collected from femur and tibia in phosphate-buffered saline (Thermo Fisher Scientific). After filtration through a 70- μ m cell strainer the cell suspension was centrifuged for 5 minutes at $300 \times g$ and the obtained cell pellet was incubated with ACK lysing buffer (BioWhittaker, Walkersville, MD) for 1 minute to

Table 2. Primers

Gene	Forward, 5'-3'	Reverse, 5'-3'
<i>Acc1</i>	TGGACAGACTGATCGCAGAGAAAG	TGGAGAGCCCCACACACA
<i>Acta2</i>	TCCTGACGCTGAAGTATCCGATA	GGTGCCAGATCTTTTCCATGTC
<i>Adgre5</i>	ATTCCACCGTCTGCAAAAACA	GGGCAGCAGTGTCCAAGTAG
<i>Atgl</i>	CCACTCACATCTACGGAGCC	TAATGTTGGCACCTGCTTCA
<i>Ccl2</i>	TCTGGACCCATTCTTCTTGG	TCAGCCAGATGCAGTTAACGC
<i>Cd36</i>	CCTGCAAATGTCAGAGGAAA	GCGACATGATTAATGGCACA
<i>Cd44</i>	TGAAACATGCAGGTATGGGT	GCTGAGGCATTGAAGCAATA
<i>Dgat1</i>	GACGGCTACTGGGATCTGA	TCACCACACACCAATTCAGG
<i>Dr5</i>	GGTCCTCTTGATGGGCTCTC	GTTGCTGCTTGCTGTGCTAC
<i>Fasn</i>	GGAGGTGGTGATAGCCGGTAT	TGGGTAATCCATAGAGCCAG
<i>F4/80</i>	TTTGGCTATGGGCTCCAGTC	GCAAGGAGGACAGAGTTTATCGTG
<i>Gapdh</i>	AGCAGCCGCATCTTCTTGTCAGTG	GGCCTTGACTGTGCCGTTGAATTT
<i>Hsl</i>	CCTGCAAGAGTATGTCACGC	GGAGAGAGTCTGCAGGAACG
<i>Icam1</i>	CAATTTCTCATGCCGCACAG	AGCTGGAAGATCGAAAAGTCCG
<i>Igfbp1</i>	ATCAGCCCATCCTGTGGAAC	TGCAGCTAATCTCTCTAGCACTT
<i>Il1b</i>	TCGCTCAGGGTCACAAGAAA	CATCAGAGGCAAGGAGGAAAAC
<i>Il6</i>	ACAAGTCGGAGGCTTAATTACACAT	TTGCCATTGCACAACCTTTTTTC
<i>Lep</i>	GAGACCCCTGTGTCGGTTC	CTGCGTGTGTGAAATGTCATTG
<i>Ly6g</i>	TGCGTTGCTCTGGAGATAGA	CAGAGTAGTGGGGCAGATGG
<i>Rbp4</i>	AGTCAAGGAGAAGCTTCGACAAGG	CAGAAAAGCTCAGCGATGATGTTG
<i>Retn</i>	AAGAACCTTTTCAATTTCCCCTCT	GTCCAGCAATTTAAGCCAATGTT
<i>S100a8</i>	AAATCACCATGCCCTCTACAAG	CCCCTTTTATCACCATCGCAA
<i>S100a9</i>	ATACTCTAGGAAGGAAGGACACC	TCCATGATGTCATTTATGAGGGC
<i>Scd1</i>	TTCTTGCGATACACTCTGGTGC	CGGGATTGAATGTTCTTGTCTGT
<i>Sele</i>	CCAATCTGAAACATTCACCGAGT	GAGTCTTTGGTTGCTTGGATGTA
<i>Sell</i>	TACATTGCCAAAAGCCCTTAT	CATCGTTCCATTTCCAGAGTC
<i>Selp</i>	GCCAGTTCATGTGCGATGAA	GGCGAAGATTCTCGGACACTT
<i>Tgfb</i>	CAACCCAGGTCCTTCTCTAAA	GGAGAGCCCTGGATACCAAC
<i>Tnfa</i>	CCCTCACACTCAGATCATCTTCT	GCTACGACGTGGGCTACAG
<i>Vcam1</i>	TGAACCCAAACAGAGGCAGAGT	GGTATCCCATCACTTGAGCAGG

remove red blood cells. The neutrophils were isolated by magnetic activated cell sorting using a Neutrophil Isolation Kit (Miltenyi Biotec, San Diego, CA) according to the manufacturer's instructions.

TSEC Culture

TSECs were kindly provided by Dr Vijay Shah (GI Research Unit, Mayo Clinic, Rochester, MN) and cultured as previously described⁵³ using Endothelial Cell Medium (Sciencell Research Laboratories, Carlsbad, CA). TSECs cultured in 24-well plates were exposed for 24 hours to palmitic acid (600 $\mu\text{mol/L}$), IL1 β (10 ng/mL), tumor necrosis factor α (50 ng/mL), transforming growth factor β (10 ng/mL), CXCL1 (100 ng/mL), or supernatant from primary hepatocytes that had been exposed previously to palmitic acid (600 $\mu\text{mol/L}$) or vehicle for 24 hours.

Co-culture of TSECs With Freshly Isolated Neutrophils

TSECs were seeded into 8-well chamber slides and cultured until 100% cell confluence was reached. The cells then were exposed for 24 hours to inflammatory triggers solubilized in culture medium (palmitic acid, 600 $\mu\text{mol/L}$; IL1 β , 20 ng/mL; and IL6, 100 ng/mL), supernatant from primary hepatocytes that had been previously exposed to palmitic acid (600 $\mu\text{mol/L}$) or vehicle for 24 hours. After medium refreshment, freshly isolated neutrophils were added (200,000 cells/well) to activated TSECs and further co-cultured for 9 hours. Hereafter, the cell supernatants were aspirated and the wells were thoroughly rinsed with phosphate-buffered saline (Thermo Fisher Scientific) to remove all nonadhered cells. Adhered neutrophils to TSEC monolayers were visualized using an Axio Vert.A1 fluorescence microscope (Zeiss).

Statistical Analysis

All data were analyzed using GraphPad Prism software (v. 5.0a; GraphPad Software, La Jolla, CA) and are expressed as the means \pm SEM. A Student *t* test was performed to compare values obtained from 2 groups and a 1-way analysis of variance, followed by the Tukey or Fisher post hoc test, was used to compare values obtained from 3 groups. Results with a *P* value less than .05 were considered significantly different.

References

- Friedman SL, Neuschwander-Tetri BA, Rinella M, Sanyal AJ. Mechanisms of NAFLD development and therapeutic strategies. *Nat Med* 2018;24:908–922.
- Zhou J, Zhou F, Wang W, Zhang XJ, Ji YX, Zhang P, She ZG, Zhu L, Cai J, Li H. Epidemiological features of NAFLD from 1999 to 2018 in China. *Hepatology* 2020; 71:1851–1864.
- Estes C, Razavi H, Loomba R, Younossi Z, Sanyal AJ. Modeling the epidemic of nonalcoholic fatty liver disease demonstrates an exponential increase in burden of disease. *Hepatology* 2018;67:123–133.
- Younossi ZM, Koenig AB, Abdelatif D, Fazel Y, Henry L, Wymer M. Global epidemiology of nonalcoholic fatty liver disease—meta-analytic assessment of prevalence, incidence, and outcomes. *Hepatology* 2016;64:73–84.
- Chang B, Xu MJ, Zhou Z, Cai Y, Li M, Wang W, Feng D, Bertola A, Wang H, Kunos G, Gao B. Short- or long-term high-fat diet feeding plus acute ethanol binge synergistically induce acute liver injury in mice: an important role for CXCL1. *Hepatology* 2015;62:1070–1085.
- Hwang S, He Y, Xiang X, Seo W, Kim S, Ma J, Ren T, Park SH, Zhou Z, Feng D, Kunos G, Gao B. Interleukin-22 ameliorates neutrophil-driven nonalcoholic steatohepatitis through multiple targets. *Hepatology* 2020; 72:412–429.
- He Y, Hwang S, Cai Y, Kim SJ, Xu M, Yang D, Guillot A, Feng D, Seo W, Hou X, Gao B. MicroRNA-223 ameliorates nonalcoholic steatohepatitis and cancer by targeting multiple inflammatory and oncogenic genes in hepatocytes. *Hepatology* 2019;70:1150–1167.
- Tran A, Gual P. Non-alcoholic steatohepatitis in morbidly obese patients. *Clin Res Hepatol Gastroenterol* 2013; 37:17–29.
- Du Plessis J, Van Pelt J, Korf H, Mathieu C, Van Der Schueren B, Lannoo M, Oyen T, Topal B, Fetter G, Nayler S, Van Der Merwe T, Windmolders P, Van Gaal L, Verrijken A, Hubens G, Gericke M, Cassiman D, Francque S, Nevens F, Van Der Merwe S. Association of adipose tissue inflammation with histologic severity of nonalcoholic fatty liver disease. *Gastroenterology* 2015; 149:635–648.
- Ley K, Laudanna C, Cybulsky MI, Nourshargh S. Getting to the site of inflammation: the leukocyte adhesion cascade updated. *Nat Rev Immunol* 2007;7:678–689.
- Vestweber D, Blanks JE. Mechanisms that regulate the function of the selectins and their ligands. *Physiol Rev* 1999;79:181–213.
- Luscinskas FW, Gimbrone MA. Endothelial-dependent mechanisms in chronic inflammatory leukocyte recruitment. *Ann Rev Med* 1996;47:413–421.
- Katayama Y, Hidalgo A, Chang J, Peired A, Frenette PS. CD44 is a physiological E-selectin ligand on neutrophils. *J Exp Med* 2005;201:1183–1189.
- Bertola A, Park O, Gao B. Chronic plus binge ethanol feeding synergistically induces neutrophil infiltration and liver injury in mice: a critical role for E-selectin. *Hepatology* 2013;58:1814–1823.
- Wang S, Song R, Wang Z, Jing Z, Wang S, Ma J. S100A8/A9 in inflammation. *Front Immunol* 2018;9:1298.
- Kraakman MJ, Lee MKS, Al-Sharea A, Dragoljevic D, Barrett TJ, Montenont E, Basu D, Heywood S, Kammoun HL, Flynn M, Whillas A, Hanssen NMJ, Febbraio MA, Westein E, Fisher EA, Chin-Dusting J, Cooper ME, Berger JS, Goldberg IJ, Nagareddy PR, Murphy AJ. Neutrophil-derived S100 calcium-binding proteins A8/A9 promote reticulated thrombocytosis and atherogenesis in diabetes. *J Clin Invest* 2017; 127:2133–2147.
- Pruenster M, Vogl T, Roth J, Sperandio M. S100A8/A9: from basic science to clinical application. *Pharmacol Ther* 2016;167:120–131.
- Ryckman C, Vandal K, Rouleau P, Talbot M, Tessier PA. Proinflammatory activities of S100: proteins S100A8,

- S100A9, and S100A8/A9 induce neutrophil chemotaxis and adhesion. *J Immunol* 2003;170:3233–3242.
19. Nacken W, Roth J, Sorg C, Kerkhoff C. S100A9/S100A8: myeloid representatives of the S100 protein family as prominent players in innate immunity. *Microsc Res Tech* 2003;60:569–580.
 20. Schiopu A, Cotoi OS. S100A8 and S100A9: DAMPs at the crossroads between innate immunity, traditional risk factors, and cardiovascular disease. *Mediat Inflamm* 2013;2013:828354.
 21. Catalán V, Gómez-Ambrosi J, Rodríguez A, Ramírez B, Rotellar F, Valentí V, Silva C, Gil MJ, Fernández-Real JM, Salvador J, Frühbeck G. Increased levels of calprotectin in obesity are related to macrophage content: Impact on inflammation and effect of weight loss. *Mol Med* 2011;17:1157–1167.
 22. Serhal R, Hilal G, Boutros G, Sidaoui J, Wardi L, Ezzeddine S, Alaaeddine N. Nonalcoholic steatohepatitis: Involvement of the telomerase and proinflammatory mediators. *Biomed Res Int* 2015;2015:850246.
 23. Björk P, Björk A, Vogl T, Stenström M, Liberg D, Olsson A, Roth J, Ivars F, Leanderson T. Identification of human S100A9 as a novel target for treatment of autoimmune disease via binding to quinoline-3-carboxamides. *PLoS Biol* 2009;7:e97.
 24. McDonald B, McAvoy EF, Lam F, Gill V, De La Motte C, Savani RC, Kubes P. Interaction of CD44 and hyaluronan is the dominant mechanism for neutrophil sequestration in inflamed liver sinusoids. *J Exp Med* 2008;205:915–927.
 25. Lake AD, Novak P, Fisher CD, Jackson JP, Hardwick RN, Billheimer DD, Klimecki WT, Cherrington NJ. Analysis of global and absorption, distribution, metabolism, and elimination gene expression in the progressive stages of human nonalcoholic fatty liver disease. *Drug Metab Dispos* 2011;39:1954–1960.
 26. Feldstein AE, Canbay A, Angulo P, Taniai M, Burgart LJ, Lindor KD, Gores GJ. Hepatocyte apoptosis and Fas expression are prominent features of human nonalcoholic steatohepatitis. *Gastroenterology* 2003;125:437–443.
 27. Ait Ahmed Y, Fu Y, Rodrigues RM, He Y, Guan Y, Guillot A, Ren R, Feng D, Hidalgo J, Ju C, Lafdil F, Gao B. Kupffer cell restoration after partial hepatectomy is mainly driven by local cell proliferation in IL-6-dependent autocrine and paracrine manners. *Cell Mol Immunol* 2021, Epub ahead of print.
 28. Guillot A, Guerri L, Feng D, Kim SJ, Ahmed YA, Paloczi J, He Y, Schuebel K, Dai S, Liu F, Pacher P, Kisseleva T, Qin X, Goldman D, Tacke F, Gao B. Bile acid-activated macrophages promote biliary epithelial cell proliferation through integrin $\alpha v \beta 6$ upregulation following liver injury. *J Clin Invest* 2021;131:e132305.
 29. Rada P, González-Rodríguez Á, García-Monzón C, Valverde ÁM. Understanding lipotoxicity in NAFLD pathogenesis: is CD36 a key driver? *Cell Death Dis* 2020;11:1–15.
 30. Bijnen M, Josefs T, cuijpers I, Maalsen CJ, van de gaar J, Vroomen M, Wijnands E, Rensen SS, Willem GJM, Hofker MH, Biessen E, Stehouwer CD, Schalkwijk C, Wouters K. Adipose tissue macrophages induce hepatic neutrophil recruitment and macrophage accumulation in mice. *Gut* 2018;67:1317–1327.
 31. Kim SJ, Feng D, Guillot A, Dai S, Liu F, Hwang S, Parker R, Seo W, He Y, Godlewski G, Jeong W Il, Lin Y, Qin X, Kunos G, Gao B. Adipocyte death preferentially induces liver injury and inflammation through the activation of chemokine (C-C motif) receptor 2-positive macrophages and lipolysis. *Hepatology* 2019;69:1965–1982.
 32. Frühbeck G, Méndez-Giménez L, Fernández-Formoso JA, Fernández S, Rodríguez A. Regulation of adipocyte lipolysis. *Nutr Res Rev* 2014;27:63–93.
 33. Polyzos S, Kountouras J, Zavos C. Nonalcoholic fatty liver disease: the pathogenetic roles of insulin resistance and adipocytokines. *Curr Mol Med* 2009;9:299–314.
 34. Kucukoglu O, Sowa JP, Mazzolini GD, Syn WK, Canbay A. Hepatokines and adipokines in NASH-related hepatocellular carcinoma. *J Hepatol* 2021;74:442–457.
 35. Rodríguez A, Catalán V, Frühbeck G. Metabolism and satiety. In: Blundell J, Bellisle F, eds. *Satiation, satiety and the control of food intake*. 1st ed. Sawston, United Kingdom: Elsevier, 2013:75–111.
 36. Singh S, Allen AM, Wang Z, Prokop LJ, Murad MH, Loomba R. Fibrosis progression in nonalcoholic fatty liver vs nonalcoholic steatohepatitis: a systematic review and meta-analysis of paired-biopsy studies. *Clin Gastroenterol Hepatol* 2015;13:643–654.
 37. Schuster S, Cabrera D, Arrese M, Feldstein AE. Triggering and resolution of inflammation in NASH. *Nat Rev Gastroenterol Hepatol* 2018;15:349–364.
 38. Hwang S, Wang X, Rodrigues RM, Ma J, He Y, Seo W, Park SH, Kim S, Feng D, Gao B. Protective and detrimental roles of p38 α mitogen-activated protein kinase in different stages of nonalcoholic fatty liver disease. *Hepatology* 2020;72:873–891.
 39. Simons N, Bijnen M, Wouters KAM, Rensen SS, Beulens JWW, van Greevenbroek MMJ, 't Hart LM, Greve JWM, van der Kallen CJH, Schaper NC, Schalkwijk CG, Stehouwer CDA, Brouwers MCGJ. The endothelial function biomarker soluble E-selectin is associated with nonalcoholic fatty liver disease. *Liver Int* 2020;40:1079–1088.
 40. Flach RJR, Matevossian A, Akie TE, Negrin KA, Paul MT, Czech MP. $\beta 3$ -adrenergic receptor stimulation induces e-selectin-mediated adipose tissue inflammation. *J Biol Chem* 2013;288:2882–2892.
 41. Musso G, Gambino R, Bo S, Uberti B, Biroli G, Pagano G, Cassader M. Should nonalcoholic fatty liver disease be included in the definition of metabolic syndrome? A cross-sectional comparison with Adult Treatment Panel III criteria in nonobese nondiabetic subjects. *Diabetes Care* 2008;31:562–568.
 42. Velázquez KT, Enos RT, Bader JE, Sougiannis AT, Carson MS, Chatzistamou I, Carson JA, Nagarkatti PS, Nagarkatti M, Murphy EA. Prolonged high-fat-diet feeding promotes non-alcoholic fatty liver disease and alters gut microbiota in mice. *World J Hepatol* 2019;11:619–637.
 43. Ivetic A, Green HLH, Hart SJ. L-selectin: a major regulator of leukocyte adhesion, migration and signaling. *Front Immunol* 2019;10:1068.

44. Liu Z, Yago T, Zhang N, Panicker SR, Wang Y, Yao L, Mehta-D'souza P, Xia L, Zhu C, Mcever RP. L-selectin mechanochemistry restricts neutrophil priming in vivo. *Nat Commun* 2017;8:1–14.
45. Drescher HK, Schippers A, Rosenhain S, Gremse F, Bongiovanni L, Bruin A de, Eswaran S, Gallage SU, Pfister D, Szydłowska M, Heikenwalder M, Weiskirchen S, Wagner N, Trautwein C, Weiskirchen R, Kroy DC. L-selectin/CD62L is a key driver of non-alcoholic steatohepatitis in mice and men. *Cells* 2020;9:1106.
46. Yilmaz Y, Ulukaya E, Atug O, Dolar E. Serum concentrations of human angiopoietin-like protein 3 in patients with nonalcoholic fatty liver disease: association with insulin resistance. *Eur J Gastroenterol Hepatol* 2009; 21:1247–1251.
47. Martínez-Castillo M, Rosique-Oramas D, Medina-Avila Z, Luis Pérez-Hernández J, Higuera-De La Tijera F, Santana-Vargas D, Montalvo-Jave EE, Sanchez-Avila Francico, Torre A, Kershenobich D, Gutierrez-Reyes G. Differential production of insulin-like growth factor-binding proteins in liver fibrosis progression. *Mol Cell Biochem* 2020; 469:65–75.
48. Hagström H, Stål P, Hultcrantz R, Brismar K, Ansurudeen I. IGFBP-1 and IGF-I as markers for advanced fibrosis in NAFLD—a pilot study. *Scand J Gastroenterol* 2017;52:1427–1434.
49. Hessian PA, Edgeworth J, Hogg N. MRP-8 and MRP-14, two abundant Ca(2+)-binding proteins of neutrophils and monocytes. *J Leukoc Biol* 1993;53:197–204.
50. Zhang J, Zhao Y, Xu C, Hong Y, Lu H, Wu J, Chen Y. Association between serum free fatty acid levels and nonalcoholic fatty liver disease: a cross-sectional study. *Sci Rep* 2014;4:1–6.
51. Malhi H, Gores GJ. Molecular mechanisms of lipotoxicity in nonalcoholic fatty liver disease. *Semin Liver Dis* 2008; 28:360–369.
52. Alkhouri N, Dixon LJ, Feldstein AE. Lipotoxicity in nonalcoholic fatty liver disease: not all lipids are created equal. *Exp Rev Gastroenterol Hepatol* 2009;3:445–451.
53. Huebert RC, Jagavelu K, Liebl AF, et al. Immortalized liver endothelial cells: a cell culture model for studies

of motility and angiogenesis. *Lab Invest* 2010;90:1770–1781.

Received June 17, 2021. Accepted August 4, 2021.

Correspondence

Address correspondence to: Bin Gao, MD, PhD, Laboratory of Liver Diseases, National Institute on Alcohol Abuse and Alcoholism, National Institutes of Health, 5625 Fishers Lane, Bethesda, Maryland 20892. e-mail: bgao@mail.nih.gov; fax: (301) 480-0257.

Acknowledgements

The authors thank Dr Vijay Shah for providing the TSECs.

CRedit Authorship Contributions

Robim M Rodrigues, PhD (Conceptualization: Equal; Data curation: Lead; Formal analysis: Lead; Investigation: Lead; Methodology: Equal; Software: Lead; Visualization: Lead; Writing – original draft: Lead; Writing – review & editing: Equal)

Yong He, PhD (Conceptualization: Supporting; Formal analysis: Supporting; Investigation: Supporting; Methodology: Supporting; Writing – review & editing: Supporting)

Seonghwan Hwang, PhD (Investigation: Supporting; Writing – review & editing: Supporting)

Adeline Bertola, PhD (Formal analysis: Supporting; Writing – review & editing: Supporting)

Bryan Mackowiak, PhD (Formal analysis: Supporting; Writing – review & editing: Supporting)

Yeni Ait Ahmed (Formal analysis: Supporting)

Wonhyo Seo, PhD (Formal analysis: Supporting; Writing – review & editing: Supporting)

Jing Ma, PhD (Formal analysis: Supporting; Writing – review & editing: Supporting)

Xiaolin Wang, MD, PhD (Formal analysis: Supporting)

Seol Hee Park, PhD (Formal analysis: Supporting; Writing – review & editing: Supporting)

Yukun Guan, PhD (Formal analysis: Supporting)

Yaojie Fu (Formal analysis: Supporting)

Tamara Vanhaecke, PhD (Resources: Supporting; Writing – review & editing: Supporting)

Dechun Feng, PhD (Formal analysis: Supporting; Methodology: Supporting; Writing – review & editing: Supporting)

Bin Gao, MD, PhD (Conceptualization: Lead; Funding acquisition: Lead; Investigation: Lead; Methodology: Lead; Project administration: Lead; Resources: Lead; Supervision: Lead; Writing – original draft: Lead; Writing – review & editing: Lead)

Conflicts of interest

The authors disclose no conflicts.

Funding

Supported by the intramural program of the National Institute on Alcohol Abuse and Alcoholism, National Institutes of Health (B.G.). Also supported by fellowship 12H2219N from the Research Foundation Flanders, Belgium (R.M.R.).